13. SITE 1019[1]

Shipboard Scientific Party[2]

HOLE 1019A

Date occupied: 29 May 1996

Date departed: 29 May 1996

Time on hole: 4 hr, 15 min

Position: 41°40.969′N, 124°55.981′W

Drill pipe measurement from rig floor to seafloor (m): 991.4

Distance between rig floor and sea level (m): 11.3

Water depth (drill pipe measurement from sea level, m): 980.1

Total depth (from rig floor, m): 1001.5

Penetration (m): 10.1

Number of cores (including cores having no recovery): 1

Total length of cored section (m): 10.1

Total core recovered (m): 10.1

Core recovery (%): 100.0

Oldest sediment cored:
Depth (mbsf): 10.1
Nature: Clay with silt, diatoms, and nannofossils
Age: Quaternary

HOLE 1019B

Date occupied: 29 May 1996

Date departed: 29 May 1996

Time on hole: 0 hr, 45 min

Position: 41°40.976′N, 124°55.983′W

Drill pipe measurement from rig floor to seafloor (m): 995.4

Distance between rig floor and sea level (m): 11.3

Water depth (drill pipe measurement from sea level, m): 984.1

Total depth (from rig floor, m): 1005.5

Penetration (m): 10.1

Number of cores (including cores having no recovery): 1

Total length of cored section (m): 10.1

Total core recovered (m): 10.1

Core recovery (%): 99.0

Oldest sediment cored:
Depth (mbsf): 10.1
Nature: Clay with silt, nannofossils, foraminifers, or diatoms
Age: Quaternary

HOLE 1019C

Date occupied: 29 May 1996

Date departed: 31 May 1996

Time on hole: 1 day, 13 hr, 15 min

Position: 41°40.972′N, 124°55.975′W

Drill pipe measurement from rig floor to seafloor (m): 988.2

Distance between rig floor and sea level (m): 11.3

Water depth (drill pipe measurement from sea level, m): 976.9

Total depth (from rig floor, m): 1236.0

Penetration (m): 247.8

Number of cores (including cores having no recovery): 26

Total length of cored section (m): 247.8

Total core recovered (m): 214.0

Core recovery (%): 86.0

Oldest sediment cored:
Depth (mbsf): 247.8
Nature: Clay with silt and diatoms, silty clay
Age: Quaternary

HOLE 1019D

Date occupied: 31 May 1996

Date departed: 31 May 1996

Time on hole: 19 hr, 15 min

Position: 41°40.967′N, 124°55.979′W

Drill pipe measurement from rig floor to seafloor (m): 988.9

Distance between rig floor and sea level (m): 11.3

Water depth (drill pipe measurement from sea level, m): 977.6

Total depth (from rig floor, m): 1212.7

Penetration (m): 223.8

Number of cores (including cores having no recovery): 24

Total length of cored section (m): 223.8

Total core recovered (m): 183.0

Core recovery (%): 81.0

Oldest sediment cored:
Depth (mbsf): 223.8
Nature: Silty clay
Age: Quaternary

HOLE 1019E

Date occupied: 31 May 1996

Date departed: 1 June 1996

[1]Lyle, M., Koizumi, I., Richter, C., et al., 1997. *Proc. ODP, Init. Repts.*, 167: College Station, TX (Ocean Drilling Program).
[2]Shipboard Scientific Party is given in the list preceding the Table of Contents.

Time on hole: 10 hr, 30 min

Position: 41°40.963′N, 124°55.979′W

Drill pipe measurement from rig floor to seafloor (m): 989.5

Distance between rig floor and sea level (m): 11.3

Water depth (drill pipe measurement from sea level, m): 978.2

Total depth (from rig floor, m): 1099.0

Penetration (m): 109.5

Number of cores (including cores having no recovery): 12

Total length of cored section (m): 109.5

Total core recovered (m): 112.2

Core recovery (%): 102.0

Oldest sediment cored:
Depth (mbsf): 109.5
Nature: Silty clay
Age: Quaternary

Principal results: Site 1019 is located about 60 km west of Crescent City, California, in the Eel River Basin at a water depth of 977 mbsl. It is the nearshore drill site of the Gorda Transect. The primary drilling objective was to sample a high-resolution Pleistocene sediment section as part of the coastal transect from 30° to 40°N and as part of the Gorda Transect across the California Current at 40°N to collect information about the development of coastal upwelling as glaciation expanded in the Northern Hemisphere. It will provide important new data about organic carbon diagenesis and about minor element geochemistry through interstitial water profiles and through solid phase analyses. One of the important objectives at this site was to study the formation of the bottom-simulating reflector and to sample gas hydrates. A high-resolution interstitial water sampling program was conducted to detect evidence of gas hydrate formation and a logging program was added to measure the extent of gas hydrate formation in situ.

Five holes were cored with the APC/XCB at Site 1019 (Fig. 1) to a maximum depth of 247.8 mbsf, recovering an apparently continuous interval of Quaternary age (1.0–0.0 Ma). Holes 1019A and 1019B are 10.1-m-long failed mudline cores. Hole 1019C was cored with the APC to 74.8 mbsf and extended with the XCB to a depth of 247.8 mbsf. The hole was logged with the density-porosity combination tool string (density, neutron porosity, resistivity, and natural gamma ray), sonic-Formation MicroScanner, and the GHMT tool strings. Hole 1019D was cored with the APC to 60.6 mbsf and deepened with the XCB to 223.8 mbsf. Twelve APC cores were taken at Hole 1019E down to 109.5 mbsf. Detailed comparisons between the magnetic susceptibility and the GRAPE density record generated on the MST, and high-resolution color reflectance measured with the Oregon State University system, demonstrated complete recovery of the sedimentary sequence down to 86 mcd.

The sedimentary section begins with approximately 30 m of late Quaternary siliciclastic and biogenic sediments composed mainly of clays and silt with minor and varied amounts of diatoms and nannofossils (Fig. 1). Hemipelagic biogenic laminations are present in the uppermost 12 m. Abundant laminae and thin sand beds occur throughout the middle to lower parts of this unit. The underlying unit (196 m thick) is characterized by a predominance of siliciclastic clays and silts with a minor diatom component and absent or rare nannofossils. Laminae and thin sand beds occur only in the middle part of this unit. Sedimentation rates are extremely high (400–1000 m/m.y.) until about 800 ka. After this, rates of sedimentation drastically decreased (to about 150 m/m.y.) and further decreased to about 100 m/m.y. following 450 ka. The decreased rate of sedimentation after 800 ka probably resulted from the tectonic development of the bank immediately to the east of Site 1019, which probably blocked sediment transport from the adjacent continental shelf. Conspicuous glauconite also began to be deposited at 800 ka, simultaneously with the overall reduction in sedimentation rates, and also probably reflects formation on the developing bank. If this timing is correct, the rate of uplift of the bank is 3 cm/100 yr, a very rapid uplift rate associated with the well-known regional neotectonism.

Biostratigraphy provides limited age control for the sequence at this site. The base of Hole 1019C is dated at about 1 Ma. The middle part of the sequence is dated using the onset of the prominent 100-k.y. paleoclimatic oscillations at 800 ka and the upper part by a combination of calcareous nannofossil, radiolarian, and diatom datums. Planktonic foraminifer assemblages reflect oscillations between glacial and interglacial conditions. These faunas are marked by cooler elements during both glacial and interglacial episodes, compared to Sites 1010 to 1018 to the south. Radiolarians are completely dominated by subarctic forms, while diatoms are dominated by cool, high latitude, north Pacific assemblages, with limited subtropical forms. Radiolarian and diatom taxa characteristic of upwelling are inconspicuous at this site, and diatom assemblages contain rare but pervasive coastal planktonic forms. Benthic foraminifer assemblages indicate the presence of relatively low oxygen concentrations in bottom waters throughout the entire sequence. Intervals marked by particularly low oxygen levels occur in the uppermost part of the sequence (<250 ka).

Positive paleomagnetic inclinations of the top 75 mbsf represent most likely the Brunhes Chron. Below this depth, XCB coring disturbance prevented interpretation of the inclination record.

Calcium carbonate concentrations are generally low and show a fluctuation between 0 and 9 wt%. Total organic carbon varies from 0.5 to 1.5 wt% throughout the sediment section. The organic fraction mainly consists of marine-derived material. The most striking features of the chemical gradients in the interstitial waters are major decreases in chlorinity, salinity, and sodium with depth, which may be artifacts of methane hydrate dissociation during recovery. Other chemical gradients reflect organic matter diagenesis, the dissolution of biogenic opal, the influence of ion exchange and authigenic mineral precipitation, and the diffusive influence of reactions in underlying basalt. There are no apparent changes in the interstitial water profiles at the estimated depth of the bottom-simulating reflector.

Downhole logging did not indicate any increases in sonic velocity or density reductions that typically characterize clathrate occurrences. There was, however, an anomalously high resistivity layer at about 100 mbsf was not associated with corresponding density or velocity increases. The borehole was highly elliptical in shape with the long axis oriented north-south, consistent with borehole break-out resulting from the regional east-west maximum compressive stress orientation.

Downhole temperature measurements yield a thermal gradient of 57°C/km. Using an average measured thermal conductivity of 0.989 W/(m·K) provides a heatflow estimate of 57 mW/m^2.

BACKGROUND AND OBJECTIVES

General Description

Site 1019 is located about 60 km west of Crescent City, California, in the Eel River Basin (Fig. 2) at a water depth of 977 mbsl. It is the nearshore drill site in the Gorda Transect (40°N). The Eel River Basin is partially uplifted and extends on land south of Eureka, California. Although the earliest sediments within the basin are Miocene in age (Clarke, 1992), a thick sequence of Pleistocene sediments is found at the drill site. One of the prominent features of the western edge of the Eel River Basin is the presence of a bottom-simulating reflector (BSR; Field and Kvenvolden, 1985), which can indicate gas hydrates in the sediments above the BSR. Farther to the south, gas hydrates have been sampled with a piston core (Brooks et al., 1991). The site was surveyed in detail on the *Wecoma* cruise W9406 in 1994 and on the *Maurice Ewing* cruise EW9504 in 1995 (Lyle et al., 1995a, 1995b; Gallaway, 1997; Fig. 3). Site 1019 is located just west of an anticlinal hill in a faulted basin at the edge of the slope break over a moderately strong BSR away from recent folding where potential hydrocarbon traps could have formed.

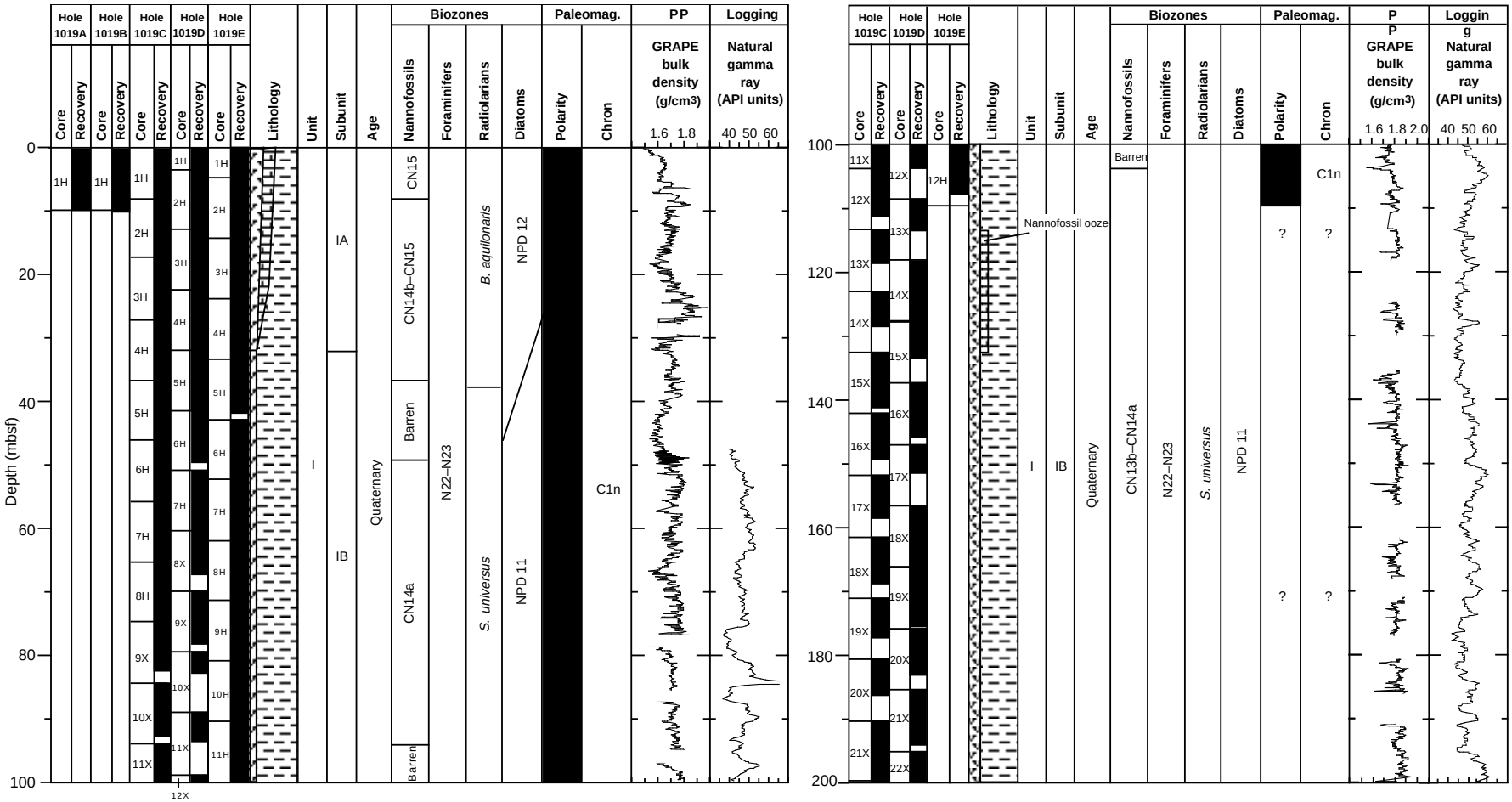

Figure 1. Site 1019 master column.

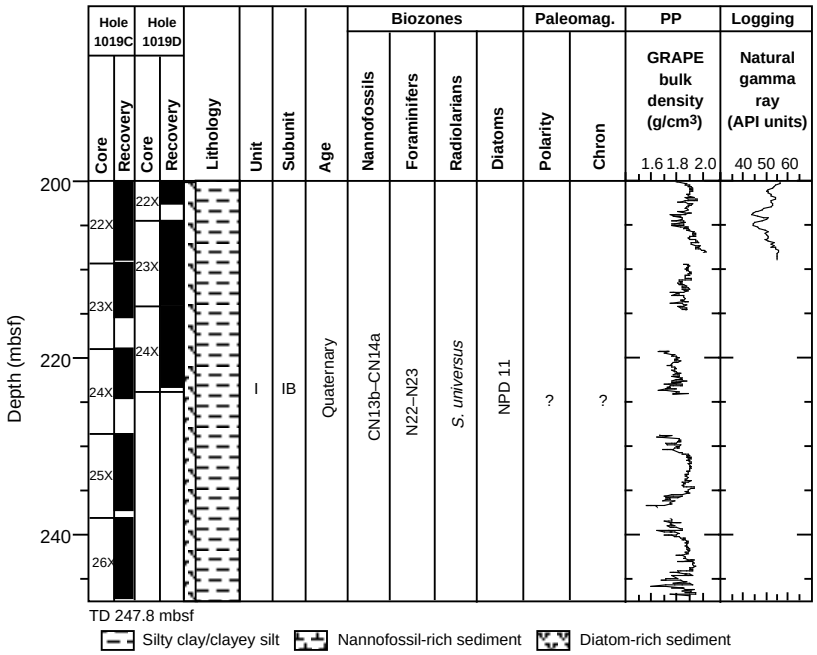

Figure 1 (continued).

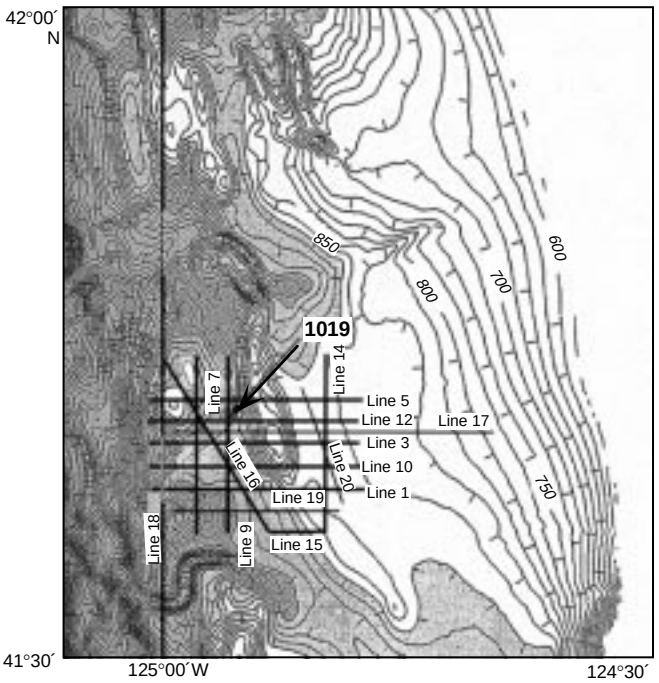

Figure 2. Location map for Site 1019, shown on NOAA swathmap bathymetry. The small hill to the east of the site is a recent anticlinal feature (Lyle et al., 1995a).

Site Objectives

At Site 1019 a high-resolution Pleistocene sediment section was drilled as part of the coastal transect from 30° to 40°N and as part of the Gorda Transect across the California Current at 40°N. It will provide important information about the development of coastal upwelling as glaciation expanded in the Northern Hemisphere. Site 1019 will also provide important new information about organic carbon diagenesis and about minor element geochemistry through interstitial water profiles and through solid phase analyses. Organic carbon content varies between 0.5% and 1.5% and appears to be of predominantly marine origin.

An important objective at this site is to study the sediment properties across the BSR and to provide evidence for the presence and concentration of gas hydrates in the sediment. A high-resolution interstitial water sampling program was conducted (one per core for the entire sediment column) to detect evidence of gas hydrate presence as dilution artifacts after recovery. A logging program was added to this site despite its relatively shallow depth to measure properties related to the concentration of gas hydrates in situ.

OPERATIONS

Transit from Site 1018 to Site 1019

The 298.0-nmi transit from Site 1018 to Site 1019 was accomplished in 43.25 hr at an average speed of 6.8 kt. The transit was made in the face of a force 8 gale storm with 16- to 18-ft seas and against a prevailing 3-kt current. A 3.5-kHz precision depth recorder survey was performed while approaching Site 1019. The *JOIDES Resolution* arrived at Site 1019 at 0730 hr on 29 May.

Hole 1019A

Hole 1019A was spudded at 1100 hr on 29 May. A full barrel prevented establishing an accurate mudline, and the hole was abandoned.

Hole 1019B

Hole 1019B was spudded at 1145 hr on 29 May. Again, a full barrel prevented the establishment of an accurate mudline, and the hole was abandoned.

Hole 1019C

Hole 1019C was spudded at 1230 hr on 29 May. APC Cores 167-1019C-1H through 8H were taken down to 74.8 mbsf with 107.1% recovery (Table 1; see Table 2 on CD-ROM in the back pocket of this volume for a more detailed coring summary). Adara temperature measurements were taken on Cores 167-1019C-4H, 6H, and 8H (see

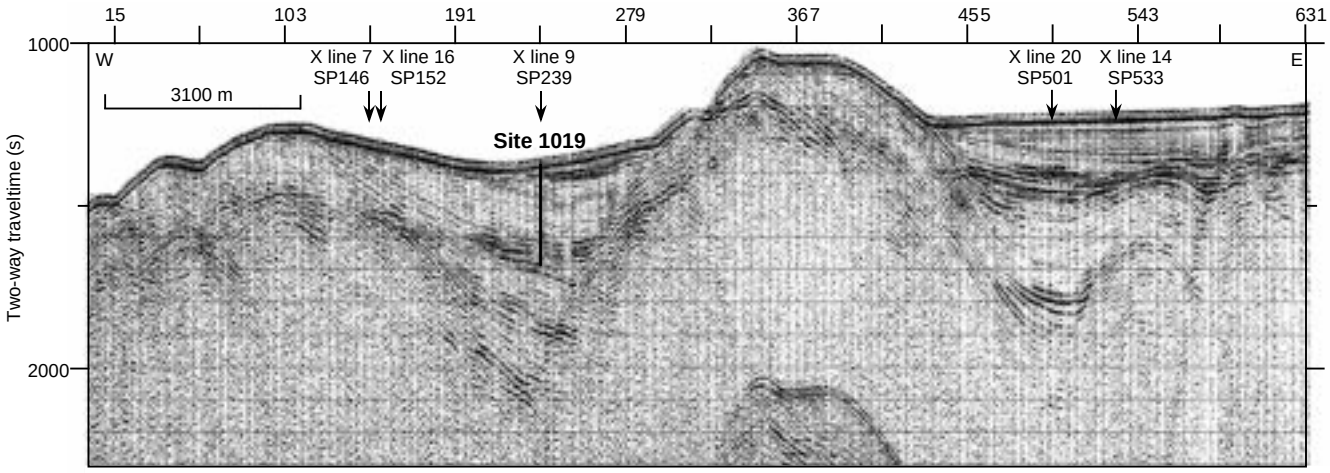

Figure 3. Seismic reflection profile through Site 1019 (Line W9406 CA1-12; Lyle et al., 1995b). The data are single-channel from an 80-in^3 water-gun source, filtered between 30 and 200 Hz. The profile cuts from west to east across the Eel River Basin and across an anticlinal hill recently folded above the surface of the basin. The site is marked by a bottom-simulating reflector (BSR) at about 200–250 ms TWT below the seafloor. On y-axis, (s) = milliseconds.

"Physical Properties" section, this chapter). XCB Cores 167-1019C-9X through 26X were taken down to 247.8 mbsf with 77.4% recovery. Gas expansion caused significant gaps in the core resulting in less than 100% core recovery. The gas was biogenic in origin and consisted mainly of methane. A 20-barrel sepiolite mud pill was circulated, and a wiper trip was performed in preparation for logging. Hole 1019C was logged with the density-porosity combination, sonic-Formation MicroScanner, and GHMT tool strings.

Hole 1019D

The vessel was offset 10 m south and Hole 1019D was spudded at 0245 hr on 31 May. APC Cores 167-1019D-1H through 7H were taken down to 60.6 mbsf with 101.3% recovery (Table 1). Oriented cores were obtained starting with Core 167-1019D-3H. XCB Cores 167-1019D-8X through 24X were taken down to 223.8 mbsf with 74.5% recovery. The reduced core recovery was caused by gas expansion similar to that in Hole 1019C.

Hole 1019E

The vessel was offset 10 m south and Hole 1019E was spudded at 2145 hr 31 May. APC Cores 167-1019E-1H through 12H were taken down to 109.5 mbsf with 102.4% recovery (Table 1). The drill string was tripped back to the surface and secured for the 8-hr transit to Site 1020 by 0730 hr on 1 June.

LITHOSTRATIGRAPHY

Introduction

A 247.8-m-thick sequence of Quaternary (~1.0–0.0 Ma) age sediment was recovered at Site 1019. Sediments are dominated by siliciclastic components, mainly clays, quartz, and feldspar. Biogenic components, predominantly diatoms and nannofossils, are important in the upper part of the section, where they form interbedded mixtures with the siliciclastic constituents. Nannofossils are a significant component only in the uppermost part of the section and in a short interval in the lower part, whereas diatoms are present throughout. Rare laminated intervals occur in the uppermost part of the sequence, otherwise, the sediment is homogeneous with rare intervals of visible bioturbation. Color changes are both subtle and gradational, usually reflecting minor lithologic variations. Laminations and thin beds of normally graded sand with sharp bases are common in the top of the section but less so in the lower half. Many of the sand layers contain glauconite. Dolomite or dolostone beds occur intermittently through the sediment sequence, and vitric ash beds are rare.

The sediments are assigned to one lithostratigraphic unit and divided into two subunits based on visual core descriptions and smear-slide estimates of composition (Fig. 4). Subunit IA is a mixed siliciclastic and biogenic unit composed mainly of clay and silt with varying amounts of diatoms and nannofossils. Abundant laminae and thin beds of sand occur throughout the middle to lower parts of this subunit. Subunit IB is composed predominantly of siliciclastic clay and silt with a minor diatom component and absent or rare nannofossils. Laminae and thin beds of sand occur primarily in the middle part of Subunit IB.

Description of Units

Unit I

Subunit IA

Hole 1019A, interval 167-1019A-1H; 0–10.1 mbsf (base of hole);
Hole 1019B, interval 167-1019B-1H; 0–10.1 mbsf (base of hole);
Hole 1019C, interval 167-1019C-1H through 3H; 0–27.3 mbsf;
Hole 1019D, interval 167-1019D-1H through 5H-2; 0–34.1 mbsf;
Hole 1019E, interval 167-1019E-1H through 4H-4; 0–30.0 mbsf.
Age: Quaternary, 0–0.3 Ma.

Subunit IA is composed of gradationally interbedded grayish olive (10Y 4/1) clay with silt and silty clay with foraminifers, and dark gray (5Y 4/1) clay diatom nannofossil silt mixed sediment and clay diatom mixed sediment with nannofossils and foraminifers. Grayish olive (10Y 4/1) diatom ooze with silt and clay occurs in the topmost 5 m. Diatom content ranges from 0% to 40% from smear-slide estimates, whereas nannofossil content ranges from 1% to 15% (also see "Organic Geochemistry" section, this chapter). XRD analyses suggest that a magnesium-rich chlorite, clinochlore, forms a significant component of the clay fraction in these sediments, particularly in gray clay-rich layers. Infrequent laminated intervals up to 0.26 m thick are present to 12 mbsf. The sediment is moderately bioturbated throughout and open, 1.0–1.5 cm diameter burrows are present to 3 mbsf. No sediment-filled burrows were observed. Abundant charcoal fragments, a few millimeters in diameter and disseminated throughout restricted sediment intervals, occur between 9–14 mbsf and at ~19.2 mbsf, 23.8 mbsf, and 27 mbsf. Laminae and thin- to medium-thick beds of dark to medium gray

Table 1. Coring summary for Site 1019.

Core	Date (1996)	Time	Top (mbsf)	Bottom (mbsf)	Length cored (m)	Length recovered (m)	Recovery (%)
167-1019A-							
1H	29 May	1815	0.0	10.1	10.1	10.11	100.1
167-1019B-							
1H	29 May	1855	0.0	10.1	10.1	10.08	99.8
167-1019C-							
1H	29 May	1940	0.0	8.3	8.3	8.32	100.0
2H	29 May	2000	8.3	17.8	9.5	10.05	105.8
3H	29 May	2030	17.8	27.3	9.5	10.24	107.8
4H	29 May	2115	27.3	36.8	9.5	10.09	106.2
5H	29 May	2200	36.8	46.3	9.5	10.31	108.5
6H	29 May	2300	46.3	55.8	9.5	9.65	101.0
7H	29 May	2340	55.8	65.3	9.5	10.82	113.9
8H	30 May	0050	65.3	74.8	9.5	10.61	111.7
9X	30 May	0145	74.8	84.5	9.7	7.64	78.7
10X	30 May	0225	84.5	94.1	9.6	8.27	86.1
11X	30 May	0300	94.1	103.7	9.6	9.57	99.7
12X	30 May	0340	103.7	113.3	9.6	7.54	78.5
13X	30 May	0430	113.3	122.9	9.6	5.28	55.0
14X	30 May	0510	122.9	132.5	9.6	5.34	55.6
15X	30 May	0550	132.5	142.1	9.6	8.61	89.7
16X	30 May	0635	142.1	151.7	9.6	7.33	76.3
17X	30 May	0730	151.7	161.3	9.6	6.79	70.7
18X	30 May	0815	161.3	170.9	9.6	7.41	77.2
19X	30 May	0910	170.9	180.5	9.6	6.30	65.6
20X	30 May	1005	180.5	190.1	9.6	5.72	59.6
21X	30 May	1110	190.1	199.7	9.6	9.37	97.6
22X	30 May	1315	199.7	209.3	9.6	9.28	96.6
23X	30 May	1500	209.3	219.0	9.7	6.06	62.5
24X	30 May	1630	219.0	228.6	9.6	5.58	58.1
25X	30 May	1730	228.6	238.2	9.6	8.68	90.4
26X	30 May	1845	238.2	247.8	9.7	9.11	94.9
167-1019D-							
1H	31 May	0950	0.0	3.6	3.6	3.60	100.0
2H	31 May	1050	3.6	13.1	9.5	10.08	106.1
3H	31 May	1100	13.1	22.6	9.5	10.14	106.7
4H	31 May	1145	22.6	32.1	9.5	10.25	107.9
5H	31 May	1230	32.1	41.6	9.5	9.25	97.3
6H	31 May	1320	41.6	51.1	9.5	8.19	86.2
7H	31 May	1410	51.1	60.6	9.5	9.89	104.0
8X	31 May	1535	60.6	70.1	9.5	6.84	72.0
9X	31 May	1615	70.1	79.6	9.5	8.26	86.9
10X	31 May	1700	79.6	89.2	9.6	3.20	33.3
11X	31 May	1750	89.2	98.9	9.7	4.40	45.3
12X	31 May	1845	98.9	108.5	9.6	5.03	52.4
13X	31 May	1920	108.5	118.1	9.6	5.00	52.1
14X	31 May	2000	118.1	127.7	9.6	9.47	98.6
15X	31 May	2040	127.7	137.3	9.6	5.77	60.1
16X	31 May	2115	137.3	146.9	9.6	8.40	87.5
17X	31 May	2205	146.9	156.5	9.6	4.49	46.8
18X	31 May	2240	156.5	166.1	9.6	9.72	101.0
19X	31 May	2320	166.1	175.7	9.6	9.34	97.3
20X	1 June	0005	175.7	185.3	9.6	7.22	75.2
21X	1 June	0100	185.3	194.9	9.6	8.56	89.1
22X	1 June	0145	194.9	204.5	9.6	7.55	78.6
23X	1 June	0225	204.5	214.2	9.7	9.45	97.4
24X	1 June	0310	214.2	223.8	9.6	8.93	93.0
167-1019E-							
1H	1 June	0445	0.0	5.0	5.0	4.93	98.6
2H	1 June	0515	5.0	14.5	9.5	10.17	107.0
3H	1 June	0535	14.5	24.0	9.5	10.14	106.7
4H	1 June	0555	24.0	33.5	9.5	10.19	107.2
5H	1 June	0620	33.5	43.0	9.5	8.47	89.1
6H	1 June	0710	43.0	52.5	9.5	10.14	106.7
7H	1 June	0755	52.5	62.0	9.5	10.53	110.8
8H	1 June	0840	62.0	71.5	9.5	10.16	106.9
9H	1 June	0925	71.5	81.0	9.5	10.00	105.2
10H	1 June	1010	81.0	90.5	9.5	10.01	105.3
11H	1 June	1050	90.5	100.0	9.5	9.58	101.0
12H	1 June	1130	100.0	109.5	9.5	7.85	82.6

Note: Table 2, on the CD-ROM in the back pocket, this volume, is a more detailed coring summary.

(N3 to N5) feldspar quartz sand occur throughout Subunit IA, predominantly between 6.5 and 13 mbsf, and 21 and 28 mbsf (Fig. 4). Some sand beds are graded and all have sharp bases. Glauconitic sand beds with quartz and feldspar occur between 22.5 and 28 mbsf, containing up to 25% glauconite. A thin bed of pale olive (10Y 6/2) dolomite occurs at Section 167-1019E-3H-5, 36 cm, and a thin bed of light gray (5Y 7/2) dolostone occurs at Section 167-1019E-4H-4, 28 cm. Vitric ash is absent from Subunit IA.

Subunit IB

Hole 1019C, interval 167-1019C-4H through 26X (base of hole); 27.3–247.8 mbsf;
Hole 1019D, interval 167-1019D-5H-3 through 24X (base of hole); 34.1–223.8 mbsf;
Hole 1019E, interval 167-1019E-4H-5 through 12H (base of hole); 30.0–109.5 mbsf.
Age: Quaternary, 0.3 to 1.0 Ma.

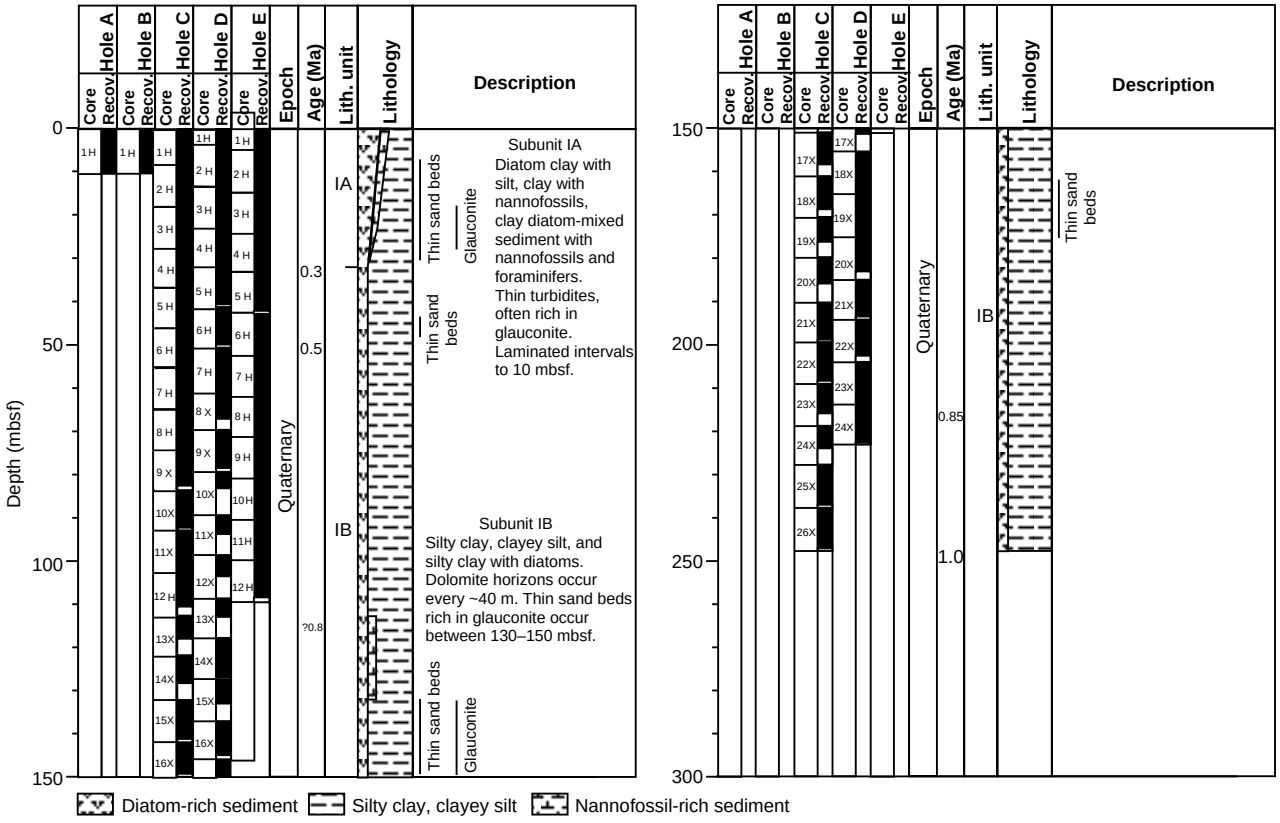

Figure 4. Site 1019 lithostratigraphic summary (0–247.8 mbsf).

The contact between Subunit IA and Subunit IB is gradational and defined texturally by the disappearance of abundant thin sand beds and compositionally by the disappearance of nannofossils from the smear-slide analyses. Subunit IB is composed of grayish olive to light grayish olive (5Y 4/1 to 10Y 5/2) clay with silt, silty clay and clayey silt, and olive gray to grayish olive (5Y 4/2 to 5Y 4/1) silty clay with diatoms, diatom clay with silt, and clay with silt and diatoms. Smear-slide estimates indicate that clay content varies from 30% to 73%, and diatom content varies from 1% to 26%. XRD analyses suggest that clinochlore is a significant component of the clay fraction, particularly in gray clay-rich layers. Lithologic contacts are gradational and reflected by subtle color changes. Sediments of Subunit IB are generally homogeneous, and visible burrows are rare. Laminae and thin beds of dark gray (N4) quartz feldspar sand with glauconite and amphibole occur between 125.5 and 165 mbsf. Most of these beds are graded and have sharp erosive bases. Amphibole content ranges between 0% and 10%, and glauconite content varies between 0% and 15% in smear-slide estimates. Rare laminae and thin beds of dark gray (N3) sandy silt occur below 165 mbsf. Thin beds and concretions of light gray (2.5Y 7/2) dolostone/dolomite occur throughout Subunit IB at approximately 40-m intervals. Two beds of light brown (5Y 7/3) to light gray (N7) vitric ash occur at approximately 27.75 and 79.3 mbsf.

Depositional History

The Quaternary sediments recovered at Site 1019 are dominated by siliciclastics with minor amounts of siliceous and calcareous biogenic components. Siliciclastic sediments with a minor diatomaceous component accumulated from about 1.0 Ma to approximately 0.8 Ma at the very high rate of 1300 m/m.y. (see "Biostratigraphy" section, this chapter). The datum for 0.8 Ma is not well constrained; however, the sedimentation rate for 1.0 Ma to 0.5 Ma would still be high at 412 m/m.y. without consideration of this datum. The apparent change in sedimentation rate at 0.8 Ma is preceded by an interval of thin, glauconite-rich sand bed deposition, which was likely deposited from turbidity currents. The glauconite-rich sands were probably shed from the top of the nearby emerging pressure ridge, 3 km to the east of Site 1019 (Gallaway, 1997). The uplift may be responsible for slowing the sediment rates by blocking direct sediment transport from the coast. Accumulation of siliciclastic-dominated sediments slowed to 220 m/m.y. at 500 ka, followed at 300 ka by a change to more biogenic-rich sedimentation, including an increase in diatom content and the emergence of nannofossils as a minor component. Glauconite-rich, thin graded sand deposits became increasingly common from ~280 to 200 ka, probably associated with continued uplift of the ridge to the east. Thin sand beds, most likely deposits from turbidity currents originating at the ridge, were deposited until approximately 100 ka, when more biogenic, hemipelagic sediments become dominant. The dolomite/dolostone beds that occur throughout the Quaternary at Site 1019 may represent brief periods of slowed deposition and increased carbonate diagenesis within the uppermost sediments.

BIOSTRATIGRAPHY

The five holes at Site 1019 recovered an apparently continuous sediment sequence of the late Quaternary. The age of the base of Hole 1019C at 248 mbsf is well constrained at ~900 ka, based on extrapolation from a radiolarian datum of known age (Fig. 5).

Both planktonic and benthic foraminifers are often common to abundant throughout Site 1019, and their preservation is usually good. Calcareous nannofossils exhibit highly variable abundance and quality of preservation and are absent in numerous samples in the

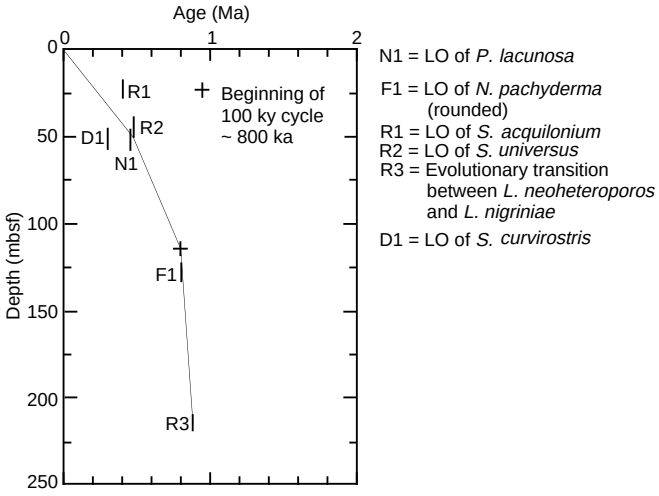

Figure 5. Age/depth plot for Hole 1019C. LO = last occurrence.

section. Radiolarians and diatoms are few to common throughout and are poorly to moderately preserved. Fine-grained sand turbidites in various parts of the sequence contain broken and well-sorted, reworked microfossil assemblages. Such samples were observed to be more common in the latest part of the sequence younger than ~400 ka (above 42 mbsf).

Biostratigraphy provides limited age control for the sequence at Site 1019. The base of Hole 1019C is well-dated, based upon an observed evolutionary transition in a radiolarian bioseries that occurred between 0.9 and 0.8 Ma (between 199.7 and 190.1 mbsf) from magnetostratigraphic intercalibration. Extrapolation from this datum provides an age of ~900 ka for the bottom of Hole 1019C. The middle part of Hole 1019C is dated by recognition of the beginning of the prominent 100 k.y. paleoclimatic oscillations at 800 ka (113 mbsf). The upper part of the sequence at Site 1019 is dated by a combination of calcareous nannofossil, radiolarian, and diatom datums. An age/depth plot (Fig. 5) based on these datums reveals extremely high sedimentation rates until ~800 ka. After this, the rates of sedimentation drastically decreased, and, following 450 ka, decreased further. The decreased rate of sedimentation after ~800 ka probably resulted from the tectonic development of the bank immediately to the east of Site 1019. Once this bank was sufficiently elevated, it would have blocked the sediment transport from the adjacent continental shelf. Conspicuous glauconite also began to be deposited at ~800 ka at the time of reduction in sedimentation rates, probably reflecting its formation on the developing bank. If this is correct, 250 m of bank uplift occurred over 800 k.y., which is 3 cm/100 yr; a very rapid rate of uplift associated with the well-known regional neotectonism (Clarke, 1992).

Planktonic foraminifer assemblages at Site 1019 clearly reflect oscillations between glacial and interglacial episodes. These faunas are marked by cooler elements during both glacial and interglacial episodes, compared with Sites 1010 to 1018 to the south. Radiolarians are completely dominated by subarctic forms, while diatoms are dominated by cool, high-latitude, north Pacific assemblages, with limited subtropical forms. Radiolarian and diatom taxa that are characteristic of upwelling are inconspicuous at Site 1019, and diatom assemblages contain rare but pervasive coastal planktonic forms.

Benthic foraminifer assemblages indicate the presence of relatively low oxygen concentrations in bottom waters throughout the entire sequence. The uppermost part of the sequence, younger than 250 ka (above 27.3 mbsf), was marked by intervals of particularly low oxygen levels. Assemblages examined from the core-catcher samples exhibit no clear relationship between changes in benthic foraminifers and glacial-interglacial oscillations as inferred from planktonic foraminifers.

Planktonic Foraminifers

Site 1019 contains an apparently continuous and generally well preserved sequence of planktonic and benthic foraminifers of middle to late Quaternary age (Table 3). The base of Hole 1019C (Sample 167-1019C-26X-CC) is less than 1.2 Ma in age, based on comparison with the Quaternary sequence of planktonic foraminifers at Site 1020, which has been magnetostratigraphically dated.

Planktonic foraminifers exhibit highly variable abundances throughout (Table 3) but are often abundant. Benthic foraminifers are usually highly abundant throughout the sequence. Preservation of both planktonic and benthic foraminifers is usually good. A number of the core-catcher samples are well-sorted, fine-grained sand turbidites that contain rare reworked planktonic foraminifers and broken and well-sorted benthic foraminifers.

The Quaternary planktonic foraminifer sequence at Site 1019 exhibits only one datum: the LO of *Neogloboquadrina pachyderma* sp. (rounded) at 133 mbsf in Hole 1019C (Sample 167-1019C-14X-CC) and 138 mbsf in Hole 1019D (Sample 167-1019D-15X-CC) with an assigned age of 0.9 Ma. Both Holes 1019C and 1019D exhibit a nearly continuous abundance of sinistrally coiled *N. pachyderma* from the base to the top of the sequence (Tables 3, 4). At Site 1020, the base of the continuous range of abundant sinistral *N. pachyderma* is dated magnetostratigraphically at ~1.2 Ma. The base of Site 1019 is thus less than 1.2 Ma.

Planktonic foraminifer assemblages at Site 1019 reflect oscillations between glacial and interglacial episodes. Glacial assemblages are of very low diversity and are completely dominated by *Globigerina bulloides* and *N. pachyderma* above 133 mbsf (Sample 167-1019C-14X-CC). Below this, *N. pachyderma* sp. (rounded) is additionally important. Interglacial assemblages exhibit much higher diversity and also include dextrally coiled *N. pachyderma, Globorotalia inflata, G. crassaformis, Globorotaloides hexagona,* and *Hastigerina aequilateralis.* At the latitude of Site 1019, even interglacial episodes are marked by a high proportion of sinistral *N. pachyderma*; dextral forms do not seem to completely dominate as during interglacial episodes in central and southern California sequences.

Benthic foraminifers at Site 1019 are dominated throughout by forms that occur widely in the relatively low-oxygen basin environments of the Southern California Borderland and the oxygen minimum zone of the California Margin. No benthic foraminifer assemblages were observed that indicate relatively highly oxygenated benthic environments at Site 1019. Faunas are generally dominated by *Uvigerina peregrina curticosta* and other forms with strong costae: *Epistominella smithi, Buliminella tenuata,* and *Bolivina spissa.* Other abundant and pervasive forms include *Cassidulina carinata, Globobulimina pacifica,* and *G. affinis, Chilostomella* spp., *Oridorsalis umbonatus,* and *Bulimina striata mexicana. Elphidium discoidale* and *Elphidium* sp. are common and well preserved in a number of samples. The quality of preservation of *Elphidium* and their occurrence with benthic foraminifer assemblages showing no evidence for reworking, suggests that these are upper bathyal representatives of an otherwise neritic benthic form. In the upper part of the sequence above ~27.3 mbsf (above Sample 167-1019C-3H-CC) the presence of abundant *Bolivina argentea* and *B. pseudobeyrichi* is inferred to reflect lower concentrations of oxygen in the benthic environment. This interval also exhibits the largest intersample benthic foraminifer changes at Site 1019. Below 156 mbsf (Sample 167-1019D-17X-CC) *Cancris* and *Pseudoparrella* are common to abundant. Faunal blooms dominated by single benthic foraminifer taxa were observed in three samples as follows: *Epistominella* in Samples 167-1019C-

Table 3. Distribution and relative abundances of planktonic foraminifers in Hole 1019C.

Zone	Core, section	Depth (mbsf)	Abundance	Preservation	*Globorotalia inflata*	*Globorotalia scitula*	*Globorotalia crassaformis*	*Neogloboquadrina humerosa*	*Neogloboquadrina* sp. "rounded"	*Neogloboquadrina pachyderma* "rounded"	*Neogloboquadrina pachyderma* 5 chambers	*Neogloboquadrina pachyderma* dex.	*Neogloboquadrina pachyderma* sin.	*Globigerina bulloides*	*Globigerina quadrilatera*	*Globigerina apertura*	*Globigerina quinqueloba*	*Globigerinita glutinata*	Sediment lithology
	167-1019C-																		
	1H-CC	8	A	M		R							A	A			A		
	2H-CC	18	A	M									A	A					
	3H-CC	27	F	P									C	C					Turbidite sand
	4H-CC	37																	Turbidite sand
	5H-CC	46	R	P									R	R					Turbidite sand
	6H-CC	56	C	M	R								A	A			A	R	
	7H-CC	65	A	G		R							A	A			C		
	8H-CC	75	A	G									A	A		F			
	9H-CC	84	A	G	F		C						A	A			C		
	10H-CC	94	F/C	G									C	C					
N22/23	11X-CC	104	B																
	12X-CC	113	A	G		F		F			C	A		A	C		C		
	13X-CC	123	C	M									A	A					
	14X-CC	133	C	G						C			A	A			C		
	15X-CC	142	R	P						R		R	R						
	16X-CC	152	R	M									R	R					
	17X-CC	161	A	G						F	R		A	A		R	F		
	18X-CC	171	A	G									A	F					
	19X-CC	181	A	G						A			A	A					
	20X-CC	190	R	G									R						
	21X-CC	200	R	P									R	R					
	22X-CC	209	A	G						A		C	A	A					
	23X-CC	219	A	G						A		F	A	A			F		
	24X-CC	229	A	G						A			A	A		R			
	25X-CC	238	B																
	26X-CC	248	A	G						C		F	A	A					

Note: See "Explanatory Notes" chapter for abbreviations.

Table 4. Coiling dominance of *Neogloboquadrina pachyderma* in Hole 1019D.

Core, section	Depth (mbsf)	*Neogloboquadrina pachyderma* coiling dominance
167-1019D-		
1H-CC	4	Sinistral/Dextral
2H-CC	13	Sinistral
3H-CC	23	(Turbidite)
4H-CC	32	Sinistral
5H-CC	42	(Turbidite)
6H-CC	51	—
7H-CC	61	Sinistral/Dextral
8X-CC	70	Sinistral
9X-CC	80	Sinistral
10X-CC	89	Sinistral/Dextral
11X-CC	99	Sinistral/Dextral
12X-CC	109	—
13X-CC	118	Sinistral
14X-CC	128	Sinistral
15X-CC	138	Sinistral
16X-CC	147	Sinistral
17X-CC	157	Sinistral
18X-CC	166	Sinistral
19X-CC	176	Sinistral
20X-CC	185	Sinistral
21X-CC	195	—
22X-CC	205	Sinistral
23X-CC	214	Sinistral
24X-CC	224	Sinistral

Note: — = insufficient data to analyze.

11X-CC and 20X-CC, and *Buliminella tenuata* in Sample 167-1019C-19X-CC (as well as at the equivalent stratigraphic level in Sample 167-1019D-19X-CC). Unlike most other sites of Leg 167, the sequence at Site 1019 lacks any clear relationships between changes in benthic foraminifer assemblages and glacial-interglacial oscillations as inferred from changes in planktonic foraminifer faunas.

Calcareous Nannofossils

Calcareous nannofossils are variable in both abundance and preservation in Holes 1019C and 1019D (Table 5). The sequence spans an interval from the Pleistocene Zone CN14a-CN13b to the Holocene Zone CN15.

Calcareous nannofossil assemblages are marked by the presence of *Emiliania huxleyi, Pseudoemiliania lacunosa, Calcidiscus leptoporus, Helicosphaera carteri,* and several morphotypes of *Gephyrocapsa* spp.

The expanded Quaternary sequence at Site 1019 allows recognition of the LO of *P. lacunosa* at 52.48 mbsf (Sample 167-1019C-6H-5, 18 cm) marking the base of Zone CN14b and with an assigned age of 460 ka.

However, at Site 1019 *P. lacunosa* is discontinuous in the upper part of its range. The presence of rare and scattered *Braarudosphaera* spp. in the sequence may have resulted from reworking of shallow-water, nearshore sediments. Reworked Paleocene and Cretaceous calcareous nannofossils are present in some samples, but are never important components of the assemblages.

Table 5. Distribution and relative abundances of calcareous nannofossils in Holes 1019A, 1019B, 1019C, and 1019D.

Zone	Core, section, interval	Depth (mbsf)	Preservation	Abundance	*Emiliania huxleyi*	*Pseudoemiliania lacunosa*	*Helicosphaera carteri*	*Gephyrocapsa oceanica* s.l.	*Gephyrocapsa* small	*Coccolithus pelagicus*	*Calcidiscus leptoporus*	*Braarudosphaera* spp.
	167-1019A-											
CN15	1H-CC	10.1	G	C	P			C	C	C		
	167-1019B-											
CN15	1H-CC	10.1	M	C	P		R	R	C	C		
	167-1019C-											
CN15	1H-CC	8.3	G	A	P			C	C	C		
CN15–CN14b	2H-CC	17.8	M	C	?			C	P	C		P
CN15–CN14b	3H-CC	27.3	P/M	R	?			P	P	F/R	R	
CN15–CN14b	4H-CC	36.8	P	RR					P			
	5H-3, 18	68.5		B								
	5H-5, 17	71.5		B								
	5H-CC	46.3		B								
	6H-3, 18	49.5		B								
CN14a	6H-5, 18	52.5	M/G	A		F/C		F	A			
CN14a	6H-CC	55.8	M/G	C		C		C	C		R	
CN14a	7H-CC	65.3	G	C/A		R	R	C	C	C		RR
CN14a	8H-3, 18	68.5	G	A		RR		C	A	R		
CN14a	8H-5, 18	71.5	M	C				C	A			
CN14a	8H-CC	74.8	M	C				F	A	F		
CN14a	9X-CC	84.3	M	C		C		C	A		C	
CN14a	10X-CC	93.9	P/M	F/C				R	A	F		
	11X-CC	103.7		B								
CN14a–CN13b	12X-CC	113.3	M	A		C			C			
CN14a–CN13b	13X-CC	122.9	M	C				R	A	C		
CN14a–CN13b	14X-CC	132.5	M	C				R	A	P		
CN14a–CN13b	15X-CC	142.1	P	RR					P	P		
	16X-CC	151.7		B								
CN14a–CN13b	17X-CC	161.3	P	R		RR				R		
	18X-CC	170.9		B								
CN14a–CN13b	19X-CC	180.5	P	RR						P		
	20X-CC	190.1		B								
	21X-CC	199.7		B								
CN14a–CN13b	22X-CC	209.3	P/M	C		RR			A	F		
CN14a–CN13b	23X-CC	219.0	M	C		P			A		C	
CN14a–CN13b	24X-CC	228.6	P	F		R					P	
	25X-CC	238.2		B								
CN14a–CN13b	26X-CC	247.9	P	R/F					P	P		
	167-1019D-											
CN15	1H-CC	3.6	G	C			R	C	C		R/F	
CN15	2H-CC	13.1	M	C	P			R	C	C		R
	3H-CC	22.6		B								
CN15–CN14b	4H-CC	32.1	G	A			R		A	F	R	R
CN15–CN14b	5H-CC	41.6	P	R				P	P			
	6H-CC	51.1		B								
CN15–CN14b	7H-CC	60.6	G	C		RR		C/F	A			
CN15–CN14b	8X-CC	70.1	M/G	C/A			R	C	A	F/C		RR
CN15–CN14b	9X-CC	79.6	G	A				C	C/A	F		RR
CN14a	10X-CC	89.2	G	A		C		F/R	A		F	
CN14a	11X-CC	98.9	P	F		F/R			P		R	
	12X-CC	108.5		B								
CN14a	13X-CC	118.1	M	C		R		F/R	A	C		
CN14a	14X-CC	127.7	M	F/C				F	C	F		
CN14a	15X-CC	137.3	P	RR				RR	R			
	16X-CC	146.9	P	RR		R						
CN14a–CN13b	17X-CC	156.5	P	R		R			P		R	
	18X-CC	166.1		B								
	19X-CC	175.7		B								
	20X-CC	185.3		B								
	21X-CC	194.9		B								
CN14a–CN13b	22X-CC	209.3	G	C/A					A	F		
CN14a–CN13b	23X-CC	214.3	G	C		P			A	C	C	
CN14a–CN13b	24X-CC	223.8	M	F/C		R			A		F	

Note: See “Explanatory Notes” chapter for abbreviations.

Diatoms

Two characteristic north Pacific diatom zones of the *Neodenticula seminae* Zone (NPD 12) to the *Simonseniella curvirostris* Zone (NPD 11) were recognized in the Quaternary section at Site 1019. Diatoms are few to common and poorly to moderately well preserved throughout the sequence. Subarctic diatom zones are not present at Site 1019 in spite of the relatively high-latitude location of this site. The relatively cold-water form *N. seminae* occurs throughout most of the sequence and is indicative of the upper Pleistocene. The typical lower Pleistocene form, *Actinocyclus oculatus*, is absent. Relatively warm-water taxa such as *Pseudoeunotia doliolus* and *Nitzschia reinholdii* are persistently present in the section except in the uppermost Zone NPD 12 (Table 6).

The last consistent occurrence of *S. curvirostris* in Sample 167-1019C-6H-CC marks the boundary between the *N. seminae* and *S. curvirostris* Zones (NPD 12/11) in Hole 1019C. This boundary in

Table 6. Distribution and relative abundances of radiolarians in Holes 1019A and 1019C.

Geologic age	North Pacific diatom zone	Numeric age (Ma)	Core, section	Sample depth (mbsf)	Abundance	Preservation	*Actinocyclus curvatulus*	*Actinocyclus lanceolatus*	*Actinocyclus oculatus*	*Actinoptychus senarius*	*Aulacosira granulata*	*Biddulphia aurita*	*Cocconeis costata*	*Cocconeis placentula*	*Coscinodiscus marginatus*	*Cymbella* sp.	*Epithemia* sp.	*Eunotia* sp.	*Hyalodiscus* sp.	*Navicula* sp.	*Neodenticula seminae*	*Nitzschia reinholdii*	*Paralia sulcata*	*Pseudoeunotia doliolus*	*Rhaphoneis* sp.	*Rhizosolenia barboi*	*Simonseniella (Rhizosolenia) curvirostris*	*Stephanodiscus astraea*	*Stephanopyxis turris*	*Thalassionema nitzschioides*	*Thalassiosira eccentrica*	*Thalassiosira nidulus*	*Thalassiosira oestrupii*	*Thalassiosira* sp.	*Thalassiothrix longissima*	Resting spores
?	?		167-1019A- 1H-CC	10.1	T	P																							T							
Quaternary	NPD 12	0.30	167-1019C- 1H-CC	8.3	T	P																							R							
			2H-CC	17.8	F	P				R													R						C							
			3H-CC	27.3	F	P	T								T						T		T						F	T	T					
			4H-CC	36.8	F	P						R									R								R							
			5H-CC	46.3	F	P					T										F								R		T					
	NPD 11		6H-CC	55.8	A	P/M	R			R								R			C			R			R		F				R			
			7H-CC	65.3	C	P/M				R							R	R			C						R	R	A	F	R			F	R	
			8H-CC	74.8	A	M/G															A					R	R	R	C						R	
			9X-CC	84.3	R	M/G															F			R					R							
			10X-CC	94.1	C	M/G			R		R							R			C						R		C	R			R			F
			11X-CC	103.7	A	M/G								R		R					A	R		R			R		C				R			
			12X-CC	113.3	R	P															R			R					R							
			13X-CC	122.9	R	P		R													R					R			C							
			14X-CC	132.5	F	P				R	R								R		R					R			C							
			15X-CC	142.1	R	P																					R		A							
			16X-CC	151.7	A	M					R										A								F							
			17X-CC	161.3	C	M				R											C	R	R			R			F							
			18X-CC	170.9	A	M					R										A	R	R				R		C		R					C
			19X-CC	180.5	F	M	R													R	R				R			C							
			20X-CC	190.1	F	M															R								C							
			21X-CC	199.7	C	P/M									R						C		R	T			R		C							F
			22X-CC	209.3	F	P															R								F							
			23X-CC	219.0	C	M															F						R		A							
			24X-CC	228.6	C	P/M						R	R		F		R				A						R		A							R
			25X-CC	238.2	C	M/G															A	R					R		C							
		<1.58	26X-CC	247.9	R	P			T																				F							

Note: See “Explanatory Notes” chapter for abbreviations.

Table 7. Distribution and relative abundances of radiolarians in Hole 1019C.

Zone	Core, section	Depth (mbsf)	Abundance	Preservation	*Actinomma popofski*	*Amphimelissa setosa*	*Botryostrobus aquilonaris*	*Botryostrobus tumidulus*	*Ceratospyris hyperborea*	*Clathrocyclas bicornis*	*Cycladophora bicincta*	*Cycladophora craspedota*	*Cycladophora d. davisiana*	*Dictyophimus crisiae*	*Lamprocyrtis neoheteroporos*	*Lamprocyrtis nigriniae*	*Lychnocanoma nipponica sakai*	*Pterocanium korotnevi*	*Siphostichoartus scalaris*	*Sphaeropyle langii*	*Spongotrochus glacialis*	*Stylacontarium acquilonium*	*Stylatractus universus*	*Stylochlamidium venustum*
	167-1019C-																							
	1H-CC	8.3	R	G					P		P	P	P					P		P				P
	2H-CC	17.8	C	G	P	P	P		P		P		P	P		P	P	P	P	P	P			
B. aquilonaris	3H-CC	27.3	R	M													P				P	P		
	4H-CC	36.8	B																					
	5H-CC	46.3	R	G			P						P			P					P	P	P	
	6H-CC	55.8	C	G	P	P	P		P				P	P		P	P	P	P	P	P	P	P	
	7H-CC	65.3	F	M		P					P		P			P	P			P	P		P	
	8H-CC	74.8	A	G	P					P	P		P			P	P	P		P	P			P
	9X-CC	84.3	R	M	P								P											
	10X-CC	94.1	B																					
	11X-CC	103.7	B																					
	12X-CC	113.3	R	G			P		P		P	P	P							P	P			
	13X-CC	122.9	R	P																				
	14X-CC	132.5	B																					
S. universus	15X-CC	142.1	R	M					P		P		P				P							
	16X-CC	151.7	R	G	P								P			P	P	P		P	P	P		
	17X-CC	161.3	B																					
	18X-CC	170.9	A	G			P	P	P				P	P		P	P	P	P	P	P	P	P	
	19X-CC	180.5	R	M					P		P		P	P			P						P	
	20X-CC	190.1	R	M				P			P		P											
	21X-CC	199.7	R	M						P	P		P			P	P	P				P		
	22X-CC	209.3	B																					
	23X-CC	219.0	R	M											P	P								
	24X-CC	228.6	R	G					P	P	P		P		P	P					P			
	25X-CC	238.2	C	G				P		P	P	P	P	P	P	P					P			
	26X-CC	247.9	C	G				P	P	P	P	P	P	P	P	P	P			P	P		P	

Notes: P = present; more detailed abundance information not available. See "Explanatory Notes" chapter for other abbreviations.

Hole 1019D occurs slightly higher (between Samples 167-1019D-3H-CC and 4H-CC) than in Hole 1019C. The persistent occurrence of *S. curvirostris* in the lowest part of the sequence (Samples 167-1019C-23X-CC to 25X-CC) indicates that an age of the base in Hole 1019C is younger than the first occurrence of this species at 1.58 Ma.

Radiolarians

Radiolarians are absent to abundant and moderately to well-preserved in core-catchers in Hole 1019C (Table 7). Barren intervals prevent precise location of upper Quaternary radiolarian events. The LO of *Stylacontarium acquilonium* provides an age older than 0.4 Ma for Sample 167-1019C-3H-CC (27.3 mbsf). Sample 167-1019C-5H-CC is older than 0.5 Ma (occurrence of *Stylatractus universus*). The evolutionary transition between *Lamprocyrtis neoheteroporos* and *Lamprocyrtis nigriniae* dated at 0.9 to 0.8 Ma is located between Samples 167-1019C-20X-CC and 21X-CC (190.1 to 199.7 mbsf). The base of Hole 1019C is younger than 0.9 to 1 Ma. Radiolarian faunas are of subarctic character throughout the sequence. Radiolarian species typical of upwelling waters are sparse.

PALEOMAGNETISM

At Hole 1019C, the archive halves of 8 APC cores and sections of the following 11 XCB cores were magnetically measured with the pass-through cryogenic magnetometer. After measuring the natural remanent magnetization (NRM), the sections were demagnetized with a peak alternating field (AF) of 20 mT. The archive halves of Cores 167-1019D-1H to 7H were only measured after AF demagnetization at 20 mT. The NRM intensity ranged mainly between 3 and 30 mA/m down to 174 mbsf (Fig. 6). After AF cleaning, the intensity was reduced to values between 0.2 and 3 mA/m in the APC and XCB cores. Quite likely the positive inclinations of the APC cored sections (top 75 mbsf) of Holes 1019C and 1019D (Figs. 6, 7) represent the Chron C1n (Brunhes) geomagnetic field. The declinations and inclinations of Core 167-1019C-5H scatter widely (Fig. 6) because of serious core disturbance. Core 167-1019D-5H was even more disturbed and therefore not measured. The first three sections of Core 167-1019E-5H were in good condition and measured after AF demagnetization. The magnetization in Core 167-1019E-5H had positive inclinations around 75°.

The best-preserved sections of each XCB core from Hole 1019C were measured with the cryogenic magnetometer before and after AF demagnetization at 20 mT with the aim of detecting the Brunhes/Matuyama transition. Demagnetization of these XCB cores (Fig. 6) did not reveal an interval with negative inclinations (reverse polarity). One should be very cautious of interpreting the positive inclinations of the XCB cores as a normal polarity interval belonging to the Brunhes Chron because of the drilling disturbance and magnetic overprint associated with XCB coring.

In an attempt to locate the Brunhes/Matuyama boundary in the XCB part of Hole 1019C, we demagnetized single samples taken from drilling biscuits which had only rotated around the azimuth of the core (z-axis). Twelve discrete samples from Cores 167-1019C-13X to 26X were stepwise AF demagnetized and measured with the Minispin magnetometer, because the Brunhes/Matuyama boundary likely occurs in this interval based on biostratigraphic datums (see "Biostratigraphy" section, this chapter). After removal of a steeply normal drilling-induced overprint, all samples have a stable compo-

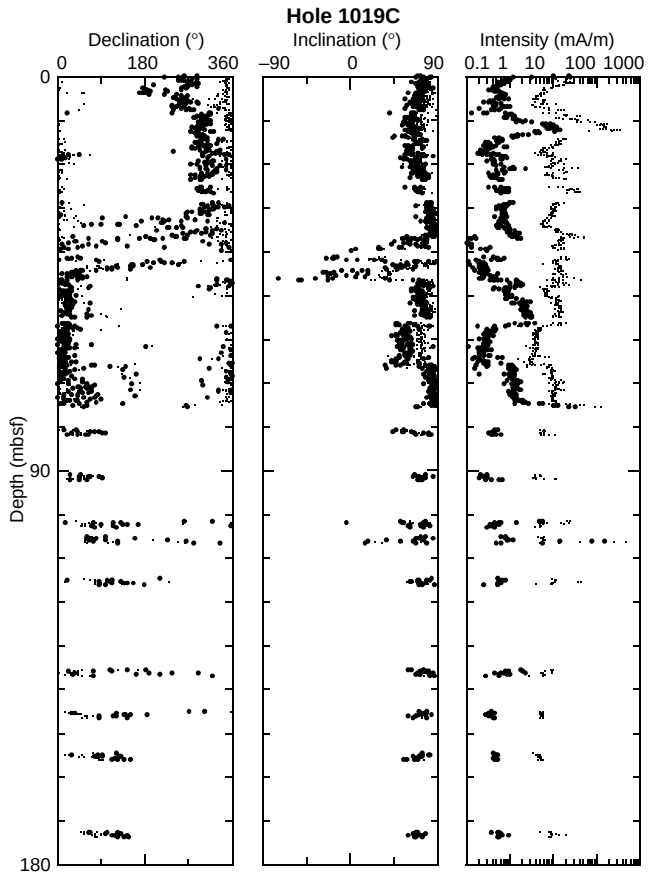

Figure 6. Plots of magnetic declination, inclination, and intensity of APC (0–75 mbsf) and XCB cores (75–174 mbsf) from Hole 1019C. Small and large dots represent the data before and after AF demagnetization at 20 mT, respectively.

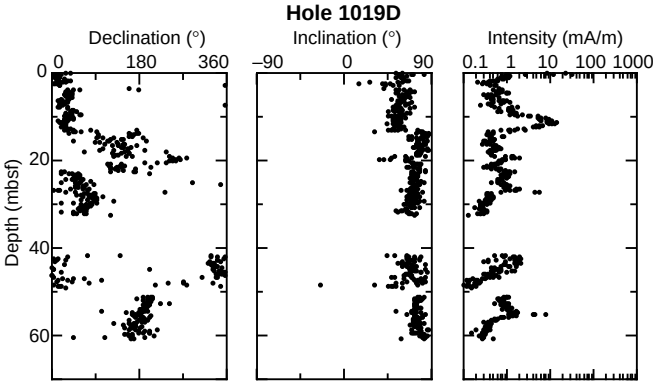

Figure 7. Plots of magnetic declination, inclination, and intensity of APC cores from Hole 1019D after AF demagnetization at 20 mT.

nent of magnetization with inclinations ranging from +50° to +70° (Table 8). Three examples of the AF demagnetization behavior of discrete samples are shown in Figure 8. Possible interpretations for this behavior are that (1) the Brunhes Chron extends from Core 167-1019C-1H to 26X; (2) a remagnetization of the gas-rich sediments in the present Earth field, when the cores expand after coring has caused

Table 8. Stepwise AF demagnetization of single specimens from Hole 1019C.

Sample	AF (mT)	Declination (°)	Inclination (°)	Intensity (mA/m)
167-1019C-				
13X-2, 13–15 cm	0	13.9	82.6	3.43
	5	358.7	72.2	0.97
	10	1.4	67.7	0.6
	20	342.8	65.8	0.34
14X-2, 16–18 cm	0	324.1	69.8	3.91
	5	293.7	71.4	1.78
	10	294.9	72.1	1.32
	20	288.7	68.3	0.8
	30	258.7	67	0.52
	40	299.2	60.6	0.45
	60	294.9	65.9	0.32
15X-3, 110–112 cm	0	12.5	43.2	2.29
	5	3.5	40.4	1.17
	10	1.6	38.6	0.85
	15	6.4	35.7	0.65
	20	4	36.1	0.56
	25	24.6	41.5	0.44
	30	28.3	31.8	0.34
	40	31.5	41.6	0.42
16X-3, 38–40 cm	0	358.4	74.2	1.99
	5	11.4	75.4	0.53
	10	12	76.4	0.32
	15	21.1	73.9	0.27
	20	46.8	68.5	0.21
	25	72	70.5	0.17
	0	90.7	55.8	0.13
17X-3, 68–70 cm	0	112.4	80.6	1.39
	5	113.7	64.4	0.47
	10	125.5	59.6	0.3
	15	118.5	50.6	0.22
	20	108.6	56.4	0.16
19X-3, 68–70 cm	0	292.3	84.8	4.67
	5	200.4	78.5	1.31
	10	202.8	73.4	0.68
	15	204.2	64	0.43
	20	224.5	60.4	0.36
	25	217.1	52.6	0.18
	30	208.2	55.6	0.19
21X-3, 111–113 cm	0	42.9	70.3	1.3
	5	61.7	61.8	1.02
	10	63.1	57.6	0.74
	15	66.9	55.3	0.66
	20	65.5	56.3	0.54
	25	64.9	56.2	0.42
	30	67.4	48.8	0.38
	40	66.8	41.8	0.27
21X-7, 21–23 cm	0	337.6	81.5	2.41
	5	20.4	75	1.09
	10	24.2	72.2	0.77
	20	31	66.6	0.55
	40	353.6	79.3	0.27
23X-2, 15–17 cm	0	95.5	85.8	2.59
	5	127.9	77.9	0.74
	10	128.2	69.8	0.39
	20	154.3	58.5	0.25
	30	123.4	51.2	0.16
24X-2, 37–39 cm	0	40.1	77.8	1.95
	5	71.8	69.7	0.64
	10	70	60.9	0.39
	0	81.6	66	0.8
	20	71.1	65.8	0.41
25X-5, 104–106 cm	0	332.7	80	1.51
	5	354.5	80.5	0.35
	10	325.1	81.4	0.25
	20	16.7	65.8	0.15
26X-7, 25–27 cm	0	261.4	83.6	6.03
	5	249.3	72.4	1.31
	10	228.6	66	0.53
	20	265	48.2	0.12

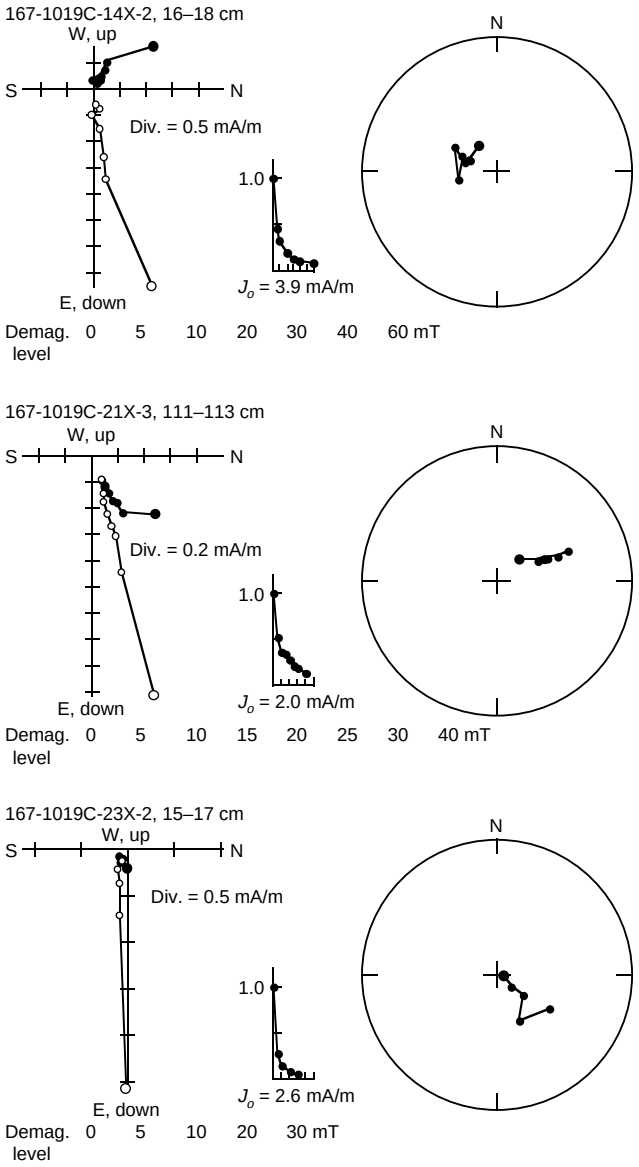

Figure 8. Alternating field demagnetization results for three of the samples listed in Table 8. Zijderveld plot (orthogonal vector projection, left), stereographic projection (right), and normalized intensity decay curves (middle) are shown for each sample. After removal of a steep overprint the remaining stable component of magnetization has positive inclination. J_o is the magnetization before AF treatment.

the magnetic grains to become realigned in the present field direction; and (3) there is drilling-induced magnetization in the XCB cores.

COMPOSITE DEPTHS AND SEDIMENTATION RATES

Multisensor track (MST) data collected at 4-cm intervals from Holes 1019A through 1019E, and color reflectance data collected at 6-cm intervals from Holes 1019C and 1019E were used to determine depth offsets in the composite section. On the composite depth scale (expressed as mcd, meters composite depth), features of the plotted MST and color reflectance data present in adjacent holes are aligned so that they occur at approximately the same depth. Working from the top of the sedimentary sequence, a constant was added to the mbsf (meters below sea floor) depth for each core in each hole to arrive at a mcd depth for that core. The depths offsets that compose the composite depth section are given in Table 9, also on CD-ROM, back pocket. The continuity of the sedimentary sequence was documented only for the upper 86 mcd.

Color reflectance was the primary parameter used for interhole correlation purposes. Magnetic susceptibility and GRAPE density measurements were used in many instances to provide additional support for composite construction. Natural gamma-ray activity measurements were made throughout the entire section in Holes 1019A,

Table 9. Site 1019 composite depth section.

Core, section	Depth (mbsf)	Offset (m)	Depth (mcd)
167-1019A-			
1H-1	0.00	2.41	2.41
167-1019B-			
1H-1	0.00	7.37	7.37
167-1019C-			
1H-1	0.00	0.00	0.00
2H-1	8.30	0.01	8.31
3H-1	17.80	0.12	17.92
4H-1	27.30	2.12	29.42
5H-1	36.80	3.09	39.89
6H-1	46.30	1.51	47.81
7H-1	55.80	1.48	57.28
8H-1	65.30	1.70	67.00
9X-1	74.80	3.86	78.66
10X-1	84.50	2.94	87.44
11X-1	94.10	2.94	97.04
12X-1	103.70	2.94	106.64
13X-1	113.30	2.94	116.24
14X-1	122.90	4.88	127.78
15X-1	132.50	5.70	138.20
16X-1	142.10	4.72	146.82
17X-1	151.70	1.68	153.38
18X-1	161.30	3.30	164.60
19X-1	170.90	3.30	174.20
20X-1	180.50	3.30	183.80
21X-1	190.10	3.30	193.40
22X-1	199.70	3.30	203.00
23X-1	209.30	3.30	212.60
24X-1	219.00	3.30	222.30
25X-1	228.60	3.30	231.90
26X-1	238.20	3.30	241.50
167-1019D-			
1H-1	0.00	0.00	0.00
2H-1	3.60	0.83	4.43
3H-1	13.10	1.63	14.73
4H-1	22.60	2.92	25.52
5H-1	32.10	4.82	36.92
6H-1	41.60	7.09	48.69
7H-1	51.10	5.12	56.22
8X-1	60.60	5.12	65.72
9X-1	70.10	6.48	76.58
10X-1	79.60	6.48	86.08
11X-1	89.20	6.48	95.68
12X-1	98.90	6.48	105.38
13X-1	108.50	6.48	114.98
14X-1	118.10	6.48	124.58
15X-1	127.70	6.48	134.18
16X-1	137.30	6.48	143.78
18X-1	156.50	6.48	162.98
19X-2	166.62	6.48	173.10
20X-1	175.70	6.48	182.18
21X-1	185.30	6.48	191.78
22X-1	194.90	6.48	201.38
23X-1	204.50	6.48	210.98
24X-1	214.20	6.48	220.68
167-1019E-			
1H-1	0.00	0.00	0.00
2H-1	5.00	–0.10	4.90
3H-1	14.50	0.27	14.77
4H-1	24.00	0.98	24.98
5H-1	33.50	1.09	34.59
6H-1	43.00	1.35	44.35
7H-2	53.03	1.43	54.46
8H-1	62.00	0.86	62.86
9H-1	71.50	4.72	76.22
10H-1	81.00	4.72	85.72
11H-1	90.50	4.72	95.22
12H-1	100.00	5.62	105.62

Note: This table is also on CD-ROM, back pocket, this volume.

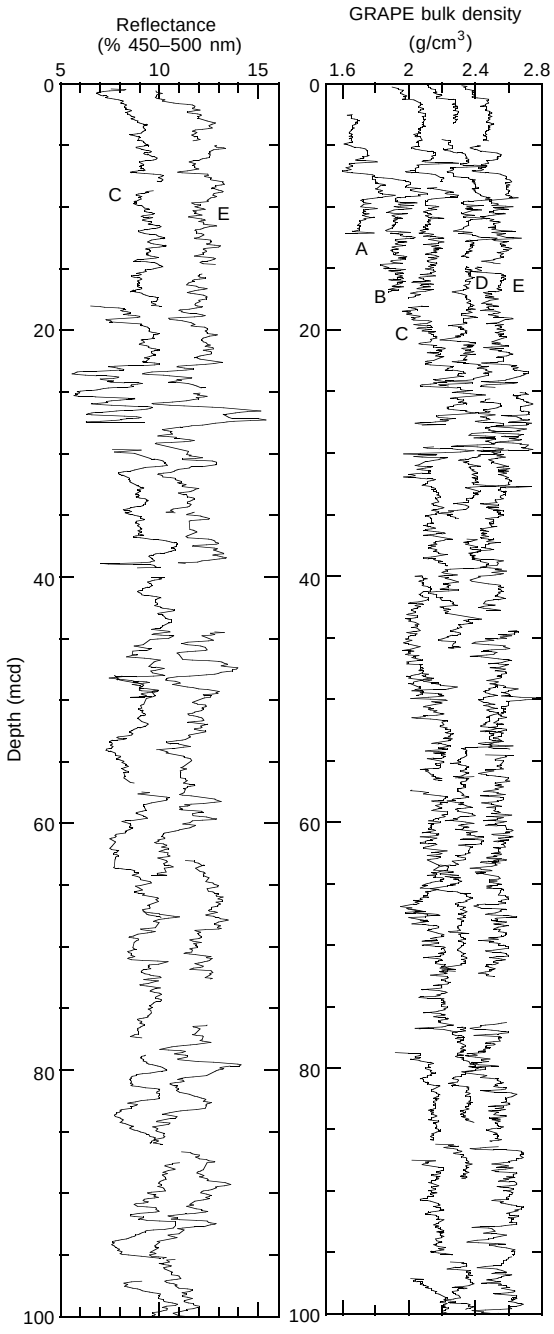

Figure 9. Smoothed (20-cm Gaussian) color reflectance (% 450–500 nm band) data for the upper 100 m from Site 1019 on the mcd scale. Holes 1019C and 1019E are vertically offset from each other by a constant (5%). Smoothed (15-cm Gaussian) GRAPE bulk density data for the upper 100 m from Site 1019 on the mcd scale. Holes 1019A, 1019B, 1019C, 1019D, and 1019E are vertically offset from each other by a constant (0.2 g/cm^3).

1019B, 1019C, and 1019D, but the sampling interval of 12 cm was insufficient for interhole correlation.

The color reflectance, magnetic susceptibility, and GRAPE records used to verify core overlap for Site 1019 are shown on a composite depth scale in Figures 9 and 10, respectively. The GRAPE data were used to identify intervals of voids and highly disturbed sediments (values less than 1.50 g/cm^3), and all MST and color reflectance data were culled from these intervals. The cores from Holes 1019A through 1019E provide nearly continuous overlap to about 86

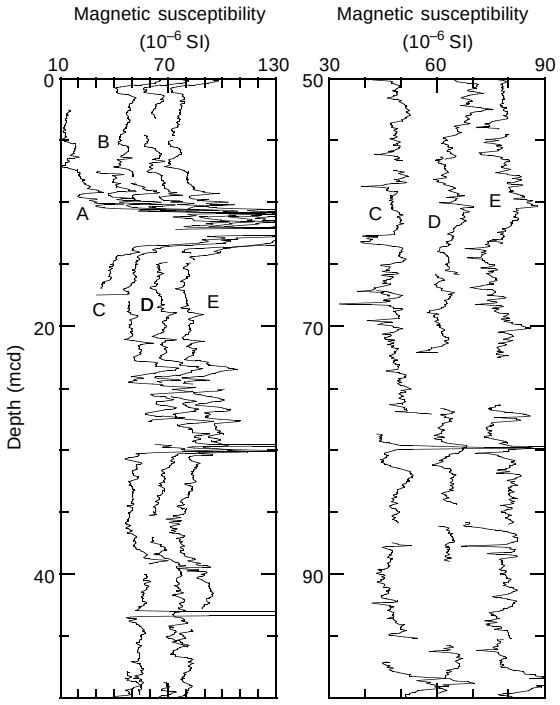

Figure 10. Smoothed (15-cm Gaussian) magnetic susceptibility data for the upper 100 m from Site 1019 on the mcd scale. Holes 1019A, 1019B, 1019C, 1019D, and 1019E are vertically offset from each other by a constant (15×10^{-6} SI). Note the different scales used for each panel.

mcd. While correlations could be made between some cores from Holes 1019C, 1019D, and 1019E below 86 mcd, there are numerous core gaps and a continuous sedimentary sequence could not be constructed from recovered cores. The composite records suggest that up to 5 m of material may be missing between cores down to about 86 mcd, although the average gap is 1–2 m. As there are no data to fill possible core gaps below 86 mcd, an assessment of core gap length below this depth is not possible.

Following construction of the composite depth section for Site 1019, a single spliced record was assembled from the aligned cores using color reflectance data where available, and magnetic susceptibility data in intervals where reflectance data were not collected. Cores from Hole 1019E were used as the backbone of the sampling splice. Cores from Holes 1019C were used to splice across core gaps in Hole 1019E. The composite depths were aligned so that tie points between adjacent holes occurred at exactly the same depths in meters composite depth. The Site 1019 splice (Table 10, also on CD-ROM, back pocket) can be used as a sampling guide to recover a single continuous sedimentary sequence down to 86 mcd. Intervals having significant disturbance or distortion were avoided if possible. In general, correlations between the cores from Holes 1019C and 1019E should be considered tentative, even in the interval where the splice was constructed. In particular, the splice tie at 40 mcd and at 77 mcd should be verified using other types of measurements.

A preliminary age model was constructed to estimate sedimentation rates (Table 11). The age model was applied to the spliced records of color reflectance, magnetic susceptibility, and GRAPE shown in Figure 11.

INORGANIC GEOCHEMISTRY

We collected 26 interstitial water samples, one from each core, from Hole 1019C at depths ranging from 4.45 to 241.84 mbsf. Chem-

Table 10. Site 1019 splice tie points.

Hole	Core, section, interval (cm)	Depth (mbsf)	Depth (mcd)		Hole	Core, section, interval (cm)	Depth (mbsf)	Depth (mcd)
1019C	1H-5, 123	7.23	7.23	tie to	1019E	2H-2, 83	7.33	7.23
1019E	2H-7, 47	14.47	14.37	tie to	1019C	2H-5, 6	14.36	14.37
1019C	2H-7, 11	16.91	16.92	tie to	1019E	3H-2, 65	16.65	16.92
1019E	3H-7, 7	23.75	24.02	tie to	1019C	3H-5, 10	23.90	24.02
1019C	3H-6, 63	25.93	26.05	tie to	1019E	4H-1, 107	25.07	26.05
1019E	4H-6, 139	32.89	33.87	tie to	1019C	4H-3, 145	31.75	33.87
1019C	4H-5, 139	34.69	36.81	tie to	1019E	5H-2, 72	35.72	36.81
1019E	5H-5, 35	39.85	40.94	tie to	1019C	5H-1, 105	37.85	40.94
1019C	5H-5, 119	43.99	47.08	tie to	1019E	6H-2, 123	45.73	47.08
1019E	6H-4, 19	47.69	49.04	tie to	1019C	6H-1, 143	47.53	49.04
1019C	6H-6, 83	54.34	55.85	tie to	1019E	7H-2, 139	54.42	55.85
1019E	7H-7, 35	60.88	62.31	tie to	1019C	7H-5, 1	60.83	62.31
1019C	7H-7, 135	65.17	66.65	tie to	1019E	8H-3, 79	65.79	66.65
1019E	8H-6, 139	70.89	71.75	tie to	1019C	8H-4, 131	70.05	71.75
1019C	8H-8, 51	75.25	76.95	tie to	1019E	9H-1, 873	72.18	76.95
1019E	9H-7, 75	81.25	85.97					

Note: This table is also on CD-ROM, back pocket, this volume.

Table 11. Site 1019 sedimentation rate age control points.

Event	Depth (mcd)	Age (Ma)	Sedimentation rate (mcd/m.y.)
T *P. lacunosa*	55.94	0.46	121.6
Evolutionary boundary between *L. neoheteroporos* and *L. nigriniae*	250.19	0.85	498.1

Note: T = top.

ical gradients in the interstitial waters at this site (Table 12) reflect organic matter diagenesis, the dissolution of biogenic opal, the influence of ion exchange and authigenic mineral precipitation reactions, and the diffusive influence of reactions in the underlying basalt. The most striking features are the major decreases in chlorinity, salinity, and sodium concentrations with depth, which may be artifacts of methane hydrate dissociation during recovery. The interstitial water profiles show no apparent changes at the estimated depth of the bottom simulating reflector (~190–210 mbsf using an interval velocity between 1550 and 1750 m/s).

Chlorinity decreases by 35% from 541 mM at 4.45 mbsf to an average of 357 mM from 154.65 to 241.84 mbsf (Fig. 12). Salinity, measured refractively as total dissolved solids, also decreases from 34 at 4.45 mbsf to 25–26 from 154.65 to 241.85 mbsf, showing a pattern similar to the chloride profile. Sodium concentrations measured by flame emission spectrophotometry were on average <2% higher than those estimated by charge balance (Table 12).

Sodium concentrations by charge balance decreased from 479 mM at 4.45 mbsf to an average of 347 mM from 154.65 to 241.85 mbsf. Alkalinity has a steep initial increase to around 43 mM from 12.75 to 41.25 mbsf, then increases to peak values >95 mM from 77.75 to 146.55 mbsf, and then decreases with depth to around 60 mM from 226.16 to 241.84 mbsf (Fig. 12). Sulfate concentrations are greater than the detection limit (~0.5 mM) in only the shallowest sample at 4.45 mbsf. Phosphate concentrations increase to strikingly high maximum values between >340 and 400 µM from 60.77 to 136.93 mbsf, with these maximum phosphate concentrations generally coincident with maximum alkalinity values. Phosphate concentrations then decrease with increasing depth to 52 µM at 241.84 mbsf. Ammonium concentrations increase with increasing depth to >13 mM by 165.11 mbsf, with relatively low ammonium concentrations relative to phosphate concentrations for this site compared to the other Leg 167 sites.

Dissolved silicate concentrations, relatively high in the shallowest samples, increase with depth to values >1000 µM from 41.25 to 50.46 mbsf, decrease slightly to values around 950 µM, and then increase again to values >1000 µM by 116.25 mbsf (Fig. 12), indicative of the dissolution of biogenic opal. Strontium concentrations decrease initially with depth to values ≤60 µM from 31.75 to 98.55 mbsf, then increase to values around seawater values at 241.84 mbsf.

Calcium concentrations decrease to a minimum of <1 mM at 41.25 mbsf, then increase with increasing depth to 4.0 mM in the deepest sample at 241.84 mbsf (Fig. 12). The average calcium gradient from 116.25 to 241.84 mbsf is +1.5 mM/100 m. Magnesium concentrations decrease substantially with increasing depth to a minimum of 25.3 mM at 41.25 mbsf coincident with the calcium minimum, then increase to values of 37–39 mM from 68.69 to 183.01 mbsf, followed by a decrease to 31.5 mM at 241.85 mbsf, with an average gradient from 116.25 to 241.84 mbsf of –5.9 mM/100 m. The decreases in dissolved calcium and magnesium in the upper sediment indicates that authigenic mineral precipitation may be significant in influencing these profiles in this depth range, while both profiles apparently reflect the diffusive influence of reactions in underlying basalt at deeper depths. At depths ≥116.25 mbsf, the calcium increase is linearly correlated to the magnesium decrease, with $\Delta Ca/\Delta Mg$ of –0.24 ($R^2 = 0.87$). Potassium concentrations generally decrease with increasing depth to values around 8 mM from 173.85 to 241.84 mbsf (Table 12). Lithium concentrations are below typical seawater values from 4.45 to 22.75 mbsf, then increase with increasing depth to 58 µM at 241.84 mbsf (Fig. 12).

ORGANIC GEOCHEMISTRY

The organic geochemistry analyses performed at Site 1019 included elemental composition, volatile hydrocarbons, and heavy hydrocarbons. Instrumentation and analytical procedures are described in the "Organic Geochemistry" section of the "Explanatory Notes" chapter, this volume.

Volatile Hydrocarbons

Volatile gases (methane, ethane, and propane) were routinely measured in the sediments of Hole 1019C as part of the shipboard safety and pollution prevention monitoring program. The results are displayed in Figure 13 and Table 13. Headspace methane concentration increases to 30,000 ppm after the second core. Below 10 mbsf, the concentration is constantly high with generally little fluctuation. Higher values (e.g., ~62 mbsf) are caused by variations in the headspace sampling technique, which is highly influenced by the volume of sediment taken from the core at the catwalk. At about 30 mbsf, the first gas voids occurred and vacutainer gas samples were taken. Vacutainer methane concentrations varied around 100%. Downcore, increasing amounts of ethane (23 ppm) and propane (10 ppm) were recorded, which resulted in methane/ethane ratios (C_1/C_2) ratios of about 450 in the lowest part of the core. The C_1/C_2 of headspace and vacutainer samples show almost the same downcore pattern. Although the values are low, no evidence of migrated higher hydrocarbons could be detected. Thus, the methane gas is probably derived by biogenic and thermogenic degradation of in situ organic material.

Elemental Analysis

We analyzed 79 sediment samples for total carbon, inorganic carbon, total nitrogen, and total sulfur. Results are presented in Table 14 (also on CD-ROM, back pocket), and Figure 14.

The percentage of calcium carbonate ($CaCO_3$) was calculated from the inorganic carbon concentrations by assuming that all carbonate occurs in the form of calcite. The concentration of $CaCO_3$ is low throughout the entire sediment column, with values between 0.3 and 9 wt%. The record can be divided into two sections according to sedimentation rates. The interval between 100 and 250 mbsf is characterized by very high constant sedimentation rates (see "Biostratig-

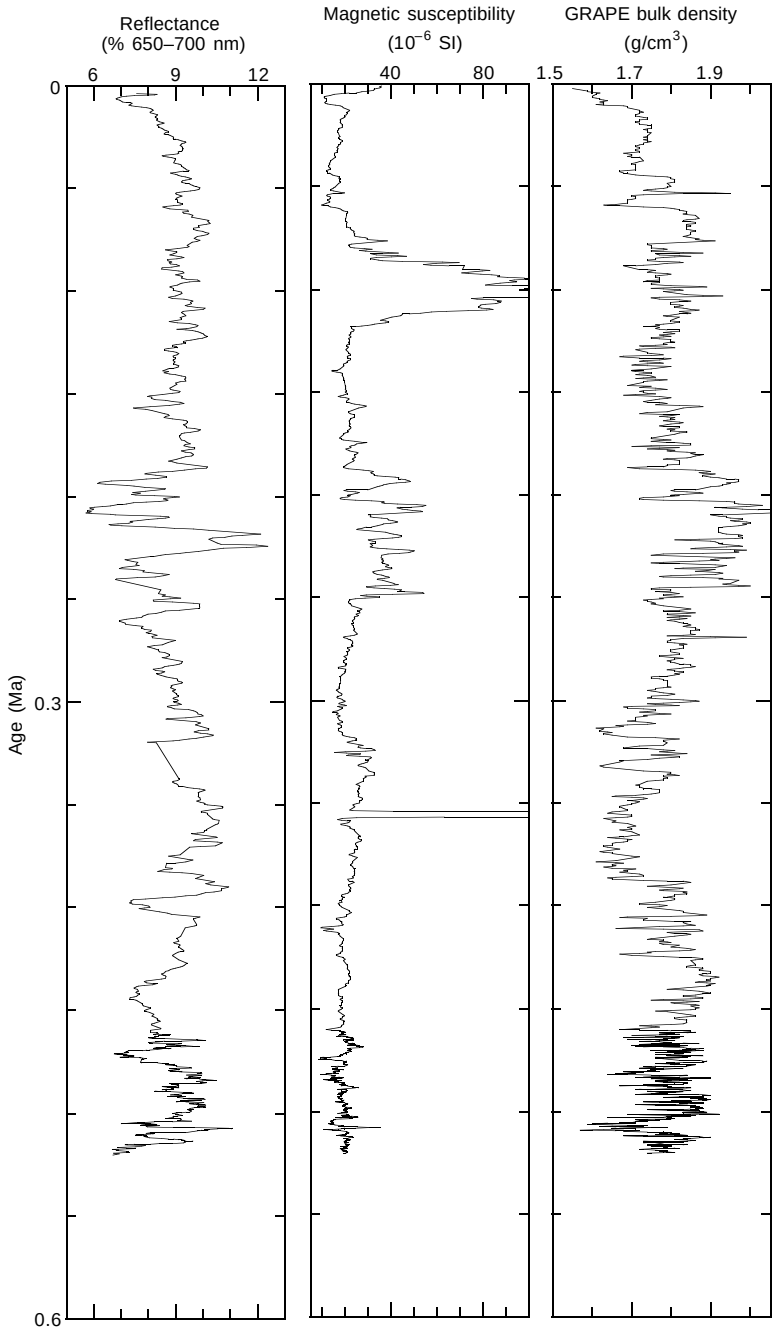

Figure 11. Spliced records of Site 1019 color reflectance, magnetic susceptibility, and GRAPE bulk density vs. age based on age control points from Table 11.

raphy" section, this chapter) and shows three well-developed carbonate cycles with a frequency of approximately 40 k.y. One reason for the cyclic deposition of calcium carbonate may be a different fluvial supply of siliciclastic material during glacial and interglacial times. This would lead to dilution-controlled rather than dissolution-controlled cycles that are consistent with well-preserved microfossils observed in sediments of Site 1019 (see "Biostratigraphy" section, this chapter). In the upper 100 mbsf, the sedimentation rate is distinctly lower and the calcium carbonate fluctuation shows no cyclic pattern. This interval (0–800 ka) is generally characterized by 100 k.y. cyclicity that is not observed using the shipboard carbonate data set.

The total organic carbon (TOC) content varies between 0.5 and 1.5 wt% with high amplitude fluctuation (Table 14; Fig. 14B). Only the uppermost sample shows a higher value, up to 2.2 wt%. Total nitrogen content varies between 0.07 and 0.25 wt%, and total sulfur content ranges from 0 to ~1.88 wt% (Table 14). To characterize the type of organic matter in the sediments, total organic carbon/total nitrogen (TOC/TN) ratios were calculated. Most of the TOC/TN ratios range between 5 and 10, which indicates a predominantly marine origin of the organic material (Bordovskiy, 1965; Emerson and Hedges, 1988).

Bitumen Analysis

Long-chain alkenones were analyzed for 32 sediment samples from 0 to 27 mbsf at Site 1019, in order to estimate paleo-sea-surface temperature (SST).

The abundances of $C_{37:2}$ and $C_{37:3}$ alkenones, U^k_{37}' values, calculated SSTs and calcium carbonate, total organic carbon, total nitrogen, and total sulfur content are shown in Table 15. The calculated SST (Fig. 15) shows a significant variation between 9.2°C and 15.4°C, which is 1°–3°C cooler than at Site 1017. As at Site 1017,

Table 12. Interstitial water geochemical data, Hole 1019C.

Core, section, interval (cm)	Depth (mbsf)	pH	Alkalinity (mM)	Salinity	Cl^- (mM)	Na^+ (mM)	SO_4^{2-} (mM)	HPO_4^{2-} (µM)	NH_4^+ (mM)	H_4SiO_4 (µM)	Ca^{2+} (mM)	Mg^{2+} (mM)	Sr^{2+} (µM)	Li^+ (µM)	K^+ (mM)
167-1019C-															
1H-3, 145–150	4.45	7.53	12.6	34.0	551	479	20.6	73	0.2	772	8.10	49.7	81	18	10.5
2H-3, 145–150	12.75	7.43	41.8	32.0	527	466	<0.5	184	2.9	680	2.99	43.5	77	10	10.2
3H-3, 145–150	22.25	7.51	43.5	30.5	502	455	<0.5	120	2.8	746	2.44	37.5	69	18	10.7
4H-3, 145–150	31.75	7.41	41.5	29.0	473	446	<0.5	147	3.2	998	1.52	27.6	57	29	10.4
5H-3, 145–150	41.25	7.30	46.7	28.0	450	434	<0.5	206	4.4	1093	0.97	25.3	53	32	10.0
6H-3, 145–150	50.46	7.48	65.4	28.0	431	424	<0.5	300	5.6	1082	1.24	30.1	53	31	9.6
7H-4, 145–150	60.77	7.78	81.7	28.5	414	413	<0.5	347	6.7	943	1.48	35.2	57	28	9.4
8H-3, 145–150	68.69	7.55	91.0	28.5	405	409	<0.5	369	7.6	932	1.64	37.0	57	28	9.2
9X-2, 145–150	77.75	7.66	98.1	33.0	399	408	<0.5	384	8.8	941	1.96	38.1	61	29	9.0
10X-3, 145–150	87.99	7.70	101	30.0	388	398	<0.5	400	9.7	954	2.16	38.8	61	30	8.8
11X-3, 145–150	98.55	7.70	96.7	30.0	366	375	<0.5	338	10.1	946	2.15	37.1	61	31	8.8
12X-3, 145–150	108.15	7.70	103	28.0	369	383	<0.5	384	10.2	995	2.16	38.3	65	32	8.9
13X-2, 145–150	116.25	7.70	103	27.0	376	388	<0.5	351	11.1	1004	2.16	38.9	65	32	8.8
14X-2, 145–150	125.85	7.78	101	27.0	363	374	<0.5	332	11.5	1012	2.32	38.6	65	32	8.6
15X-3, 145–150	136.93	7.70	98.2	26.0	354	363	<0.5	343	11.9	996	2.64	37.8	65	35	8.4
16X-3, 145–150	146.55	7.80	96.4	26.0	348	355	<0.5	325	12.4	1081	2.79	37.7	65	39	8.3
17X-2, 145–150	154.65	7.78	89.8	25.0	342	345	<0.5	269	12.6	1130	2.86	36.6	65	40	8.2
18X-3, 145–150	165.11	7.83	87.5	26.0	354	352	<0.5	275	13.1	1051	3.07	37.6	65	40	8.3
19X-2, 145–150	173.85	7.79	87.0	26.0	353	352	<0.5	237	13.4	1030	3.02	36.8	65	42	8.0
20X-2, 145–150	183.01	7.30	83.1	26.0	356	351	<0.5	228	13.6	1066	3.35	36.6	69	43	7.8
21X-4, 145–150	195.17	7.70	78.7	26.0	352	345	<0.5	220	13.4	1147	3.32	35.7	73	48	7.9
22X-3, 145–150	203.09	7.49	73.4	25.0	364	351	<0.5	147	13.4	1093	3.44	36.0	73	52	8.0
23X-3, 127–132	213.10	7.52	68.3	25.0	361	346	<0.5	144	13.1	1147	3.58	34.3	73	53	7.8
24X-3, 145–150	222.16	7.50	61.3	25.0	367	345	<0.5	106	12.4	1070	3.77	34.1	77	55	8.0
25X-3, 145–150	231.98	7.54	62.9	25.0	362	344	<0.5	70	12.5	1160	3.87	32.4	81	59	8.3
26X-3, 145–150	241.84	7.56	59.7	25.0	362	342	<0.5	52	13.0	1080	4.04	31.5	85	58	8.4

U^k_{37}' index and C_{37} alkenone abundance show somewhat similar profiles (Fig. 15). This suggests that the productivity of nannoplankton was higher in warmer periods than in cooler periods.

PHYSICAL PROPERTIES

Multisensor Track Measurements

The shipboard physical properties program at Site 1019 included nondestructive measurements of bulk density, magnetic susceptibility, *P*-wave velocity, and natural gamma-ray activity on whole sections of all cores using the MST (Fig. 16). Magnetic susceptibility was measured at 4-cm intervals at low sensitivity (1-s measuring time) on all Site 1019 cores. GRAPE bulk density measurements were made at 4-cm intervals on all Site 1019 cores. High GRAPE density values correspond well with reflections from the 3.5-kHz sub-bottom profiles (Fig. 17). Abrupt changes in GRAPE density correspond to several sandy turbidite layers (see "Lithostratigraphy" section, this chapter), feldspathic(?) and glauconitic sand, and intervals with lithic sand. PWL velocity measurements were made at 4-cm intervals on cores from Holes 1019A and 1019B and through Cores 167-1019C-3H and 167-1019D-3H, but were not run on cores from Hole 1019E. Natural gamma-ray activity was measured with a 15-s count every 12 cm on cores from Holes 1019A through 1019D and not run on cores from Hole 1019E.

Index Properties

Index properties measurements were made at one sample per working section on all cores from Hole 1019C. Values of bulk density and the index properties void ratio, porosity, water content, dry-bulk density, and grain density were determined using gravimetric Method C (Table 16 on CD-ROM in the back pocket of this volume). The data show distinct trends downhole (Fig. 18), such as an increase in bulk density values from 0 to 30 mbsf, which coincides with lithostratigraphic Subunit IA (see "Lithostratigraphy" section, this chapter). Below this, index property values are fairly constant, with sporadic fluctuations in values generally corresponding to lithologic variation. For example, below 100 mbsf there are significantly more nannofossils in the sediments and also an increase in bulk density values. Farther downhole, in the interval between 200 and 210 mbsf, bulk density values are higher, corresponding to a lack of diatoms in this interval.

Compressional-Wave Velocity

Only seven sonic velocity measurements were made in Hole 1019C with the Hamilton Frame (pair T3, x-direction) to Section 167-1019C-2H-3, beyond which high gas content (see "Organic Geochemistry" section, this chapter) attenuated the signal and precluded further velocity measurements. Values range from 1494 to 1524 m/s, averaging 1509 m/s, with one measurement of 1615 m/s at 41.76 mbsf in a sandy interval.

Heat Flow

Thermal conductivity was measured down to 78.35 mbsf in Hole 1019D (Table 17 on CD-ROM in the back pocket of this volume). Three downhole temperature measurements were taken with the APC Adara temperature tool in Hole 1019C: 5.8°C at 36.8 mbsf, 6.7°C at 55.8 mbsf, and 8.1°C at 74.8 mbsf in Cores 167-1019C-4H, 6H, and 8H, respectively (Fig. 19). Bottom-water temperature was measured on all runs, indicating a bottom-water temperature of 3.7°C ± 0.1°C. The four data points yield a thermal gradient of 57°C/km (Fig. 20). Using an average measured thermal conductivity of 0.989 W/(m·K) provides a heat-flow estimate of 57 mW/m^2 at Site 1019.

Color Reflectance

Reflectance measurements were made at 4- to 6-cm intervals for cores in Holes 1019C and 1019E. Opal content was estimated using a multiple linear regression equation generated from the Leg 167 site-survey color reflectance and opal data. To the first order, preliminary results are consistent with the lithostratigraphic units identified at Hole 1019C (Fig. 21). The highest predicted opal values occur in lithostratigraphic Subunit IA, which includes diatom clay with silt, clay with nannofossils, and clay diatom mixed sediment. In lithostratigraphic Subunit IB, which consists of primarily silty clay,

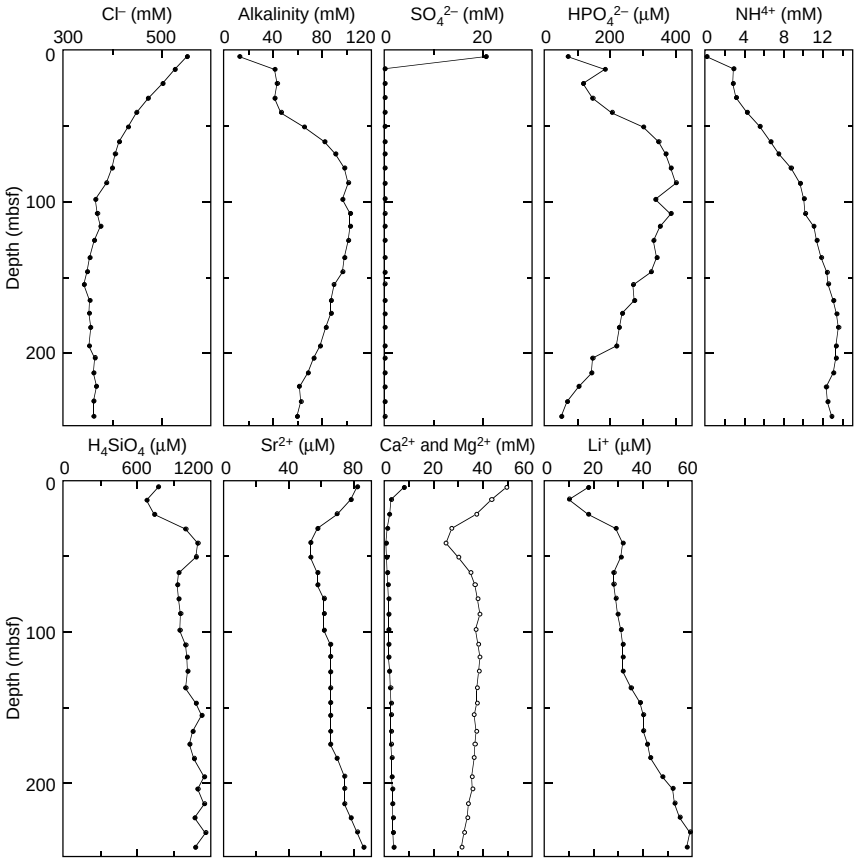

Figure 12. Interstitial water geochemical data, Site 1019. Solid circles = Ca, open circles = Mg.

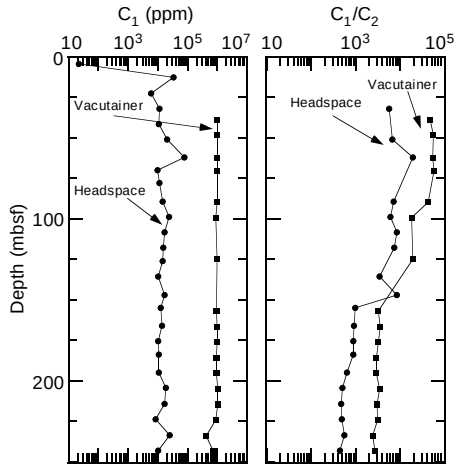

Figure 13. Depth variations of concentrations of methane (C_1) and methane/ethane (C_1/C_2) ratios obtained by the headspace and vacutainer techniques from Hole 1019C.

clayey silt, and silty clay with diatoms, predicted opal levels are generally lower.

Digital Color Video

Cores from all Site 1019 holes were imaged with the ODP color digital imaging system at 20-cm intervals downcore, providing a 0.25-mm pixel. Sediment color CIELAB L* derived from digital color or video images from Holes 1019C, 1019D, and 1019E is shown in Figure 22. Because of lighting problems, data from 0 to 100 mbsf of Hole 1019C may be offset to higher values.

DOWNHOLE MEASUREMENTS

Logging Operations and Log Quality

Hole 1019C was logged with the density-porosity combination, sonic-FMS, and GHMT tool strings. After the hole was flushed of debris and the pipe set at 65 mbsf (Table 18), the density-porosity combination tool string was lowered into the hole to conduct pass 1 (233–92 mbsf) (Fig. 23). Caliper measurements from this tool string indicate that the borehole was in poor condition, with washouts throughout the logged interval. The sonic-FMS tool string was deployed next and two passes (pass 1: 228–82 mbsf; pass 2: 226–60 mbsf) were conducted to obtain maximum image coverage of any possible clathrate features associated with the bottom-simulating reflector (BSR) observed in the seismic profiles of this site. Finally, the GHMT magnetic tool string was lowered into the hole for two complete passes (pass 1: 222–58 mbsf; pass 2: 222–70 mbsf). Sea-state conditions were calm (1-m swells), and the wireline heave compensator was used on all passes.

The TLT was run during the density-porosity tool run, but because of excessive circulation required to drill the hole and flush it of debris, the measured borehole fluid temperatures are anomalously cool.

From the orthogonal FMS caliper measurements the hole was determined to be elliptical in shape, with hole ellipticity exceeding 50% in some areas. Average minimum and maximum axes measure 14 and 12 in, respectively, with the long axis consistently oriented north-

Table 13. Concentrations of methane (C_1), ethane (C_2), and propane (C_3) obtained by the headspace and vacutainer techniques from Site 1019.

Core, section, interval (cm)	Depth (mbsf)	C_1 (ppm)	C_2 (ppm)	C_3 (ppm)	C_1/C_2
Headspace					
167-1019A-					
1H-4, 0–5	4.53	74			
167-1019B-					
1H-4, 0–5	4.53	32,591			
167-1019C-					
1H-4, 0–5	4.53	22			
2H-4, 0–5	12.83	34,425			
3H-4, 0–5	22.33	5,965			
4H-4, 0–5	31.83	11,432	2	1	5,716
5H-4, 0–5	41.33	10,832			
6H-4, 0–5	50.83	20,623	3	4	6,874
7H-5, 0–5	61.83	78,503	4	6	19,626
8H-4, 0–5	69.83	9,778			
9X-3, 0–5	77.83	11,272		2	
10X-4, 0–5	89.03	14,561	2	4	7,281
11X-4, 0–5	98.63	24,609	4	5	6,152
12X-4, 0–5	108.23	16,991	2	5	8,496
13X-3, 0–5	116.33	14,941	2	4	7,471
14X-3, 0–5	125.93	14,512		1	
15X-4, 0–5	150.53	10,383	3	3	3,461
16X-4, 0–5	146.63	16,943	2	10	8,472
17X-3, 0–5	154.73	12,887	13	4	991
18X-4, 0–5	165.83	14,010	15	3	934
19X-3, 0–5	173.93	10,575	12	2	881
20X-3, 0–5	183.53	10,601	12	2	883
21X-5, 0–5	196.13	10,879	17	4	640
22X-4, 0–5	204.23	18,780	36	7	522
23X-3, 122–127	213.78	17,428	37	8	471
24X-4, 0–5	223.53	8,587	17	4	505
25X-4, 0–5	233.13	25,624	46	9	557
26X-4, 0–5	242.73	10,387	23	6	452
Vacutainer					
167-1019C-					
4H-2, 50–51	29.31	1,289			
5H-2, 50–51	38.81	983,204	21	8	46,819
6H-2, 50–51	48.31	999,999	18	8	55,556
7H-5, 50–51	62.31	987,791	18	12	54,877
8H-4, 50–51	70.31	985,527	17	12	57,972
10X-4, 50–51	89.51	976,524	23	16	42,458
11X-4, 50–51	99.11	905,532	50	12	18,111
14X-2, 50–51	124.91	983,404	51	11	19,282
17X-4, 50–51	156.71	963,882	296	21	3,256
18X-4, 50–51	166.31	1,000,040	279	13	3,584
19X-4, 50–51	175.91	981,270	301	17	3,260
20X-4, 50–51	185.51	951,501	325	21	2,928
21X-4, 50–51	195.11	943,062	325	20	2,902
22X-4, 50–51	204.71	1,036,300	303	16	3,420
23X-4, 50–51	214.31	1,015,550	337	18	3,014
24X-4, 50–51	224.01	911,411	289	16	3,154
25X-4, 50–51	233.61	418,166	173	11	2,417
26X-4, 50–51	243.21	742,046	272	15	2,728

south throughout the hole (Fig. 24). The north-south orientation of the hole ellipticity would be consistent with orthogonal borehole break-out associated with the regional east-west compressive stress regime of this convergent margin.

Comparison of Core and Log Physical Properties Data

Because of the generally poor borehole conditions, log data quality is correspondingly poor for the measurements that require good borehole contact (principally density, neutron porosity, and FMS). An example of the influence of highly variable borehole diameter on selected log measurements at Hole 1019C is shown in Figure 25; poor contact with the borehole wall produces apparent density reductions and neutron porosity increases.

The core and log measurements of sediment bulk density are otherwise similar over their common interval, whereas the core porosity data are significantly lower than the log (neutron; APS) measurements (Fig. 25). The log porosity data are significantly higher, mainly because the neutron log porosity data reflect measurement of both free water (interstitial space) and molecularly bound water (clays and other minerals) in the formation. Hence, the neutron porosity tends to overestimate porosity in very clay rich formations such as at Hole 1019C. In addition, if clathrates exist at Site 1019 they would also cause anomalously high porosity by the methane associated gas hydrates. The density measurements from the HLDT tool can be used to estimate sediment porosity as well, using the assumption that interstitial spaces are water filled. Because this tool uses a different method for investigating formation density (gamma-ray emission from a ^{137}Cs source), it provides an alternative method to evaluate porosity. The log litho-density porosity (DPHI) measurement is thus a better measurement of porosity in these high-terrigenous-content sediments. The MST core measurements of magnetic susceptibility and natural gamma-ray activity are compared to log measurements of magnetic susceptibility and natural gamma-ray activity in Figure 26.

SUMMARY

Site 1019, located in the Eel River Basin just west of Crescent City, California, was drilled to be the nearshore site in the Gorda Transect and to study the cause of the prominent regional bottom-simulating reflector (BSR) (Fig. 27). Initial results indicate very rapid sedimentation partly controlled by active local tectonics. We did not directly identify any gas hydrates in the section, although we did see reduced chlorinities in the interstitial waters, which may be an artifact of methane hydrate decomposition during recovery. It cannot yet be confirmed that the BSR here results from the decomposition of gas hydrates within the sediment column. Five holes were drilled at the site, of which two were missed mudline cores. The site was triple cored to 110 mbsf (~0.6 Ma) and double cored to 224 mbsf (~0.8 Ma), and one hole reached 248 mbsf (~0.9 Ma). Sedimentation rates decreased radically from very high rates about 500 m/m.y. in the lower part of the section below 53 mbsf, to around 115 m/m.y. above that depth. Because of the change in sedimentation rate and the appearance of glauconite and small turbidites in the section, we hypothesize that the nearby hill to the east (Fig. 27) was uplifted at about 0.5 Ma and isolated the drill site from downslope sediment transport.

The interstitial waters at Site 1019 are significantly reduced in chlorinity, salinity, and sodium concentrations relative to normal seawater, reaching Cl^- concentrations consistently less than 65% that of normal seawater. There are no clear signals of dilution artifacts in the other interstitial water profiles, nor are there any substantial charges at the estimated depth of the BSR. The presence of methane hydrate is sometimes marked by erratically low chlorinity spikes in interstitial water as a result of methane hydrate decomposition during recovery. On Leg 164, for example, interstitial water chlorinity in methane hydrate layers was significantly lower but rarely to levels below 75% of normal seawater.

However, a chlorinity profile similar to the one at Site 1019 was observed at Sites 889/890 and interpreted to represent hydrate concentrations ranging from near zero at the seafloor to a maximum of about 35% of the pore space (Yuan, et at., 1996). Preliminary logging data are not consistent with hydrate formation. The highest resistivity zone, at about 100 mbsf, was not the zone of highest velocity as would be expected if the sediments were originally cemented by gas hydrates.

REFERENCES

Bordovskiy, O.K., 1965. Accumulation and transformation of organic substances in marine sediment, 2. Sources of organic matter in marine basins. *Mar. Geol.,* 3:5–31.

Brooks, J.M., Field, M.E., and Kennicutt, M.C., II, 1991. Observations of gas hydrates in marine sediments, offshore Northern California. *Mar. Geol.,* 96:103–108.

Clarke, S.H., Jr., 1992. Geology of the Eel River Basin and adjacent region: implications for Late Cenozoic tectonics of the Southern Cascadia subduction zone and Mendocino triple junction. *AAPG Bull.,* 76:199–224.

Emerson, S., and Hedges, J.I., 1988. Processes controlling the organic carbon content of open ocean sediments. *Paleoceanography,* 3:621–634.

Field, M.E., and Kvenvolden, K.A., 1985. Gas hydrates on the northern California continental margin. *Geology,* 13:517–520.

Gallaway, P., 1997. Three dimensional seismic modeling of Ocean Drilling Program Site 1019: implications for sedimentation, deformation, and evolution of the Eel River Basin [M.S. thesis]. Boise State University.

Lyle, M., Gallaway, P.J., Liberty, L.M., Mix, A., Stott, L., Hammond, D., Gardner, J., Dean, W., and the EW9504 Scientific Party, 1995a. Data submission. W9406 and EW9504 site surveys of the California margin proposed drillsites, Leg 167 (Vol. 1): Site maps and descriptions. Boise State Univ., *CGISS Tech. Rep.,* 95–11.

————, 1995b. Data submission. W9406 and EW9504 site surveys of the California margin proposed drillsites, Leg 167 (Vol. 2): Seismic profiles. Boise State Univ., *CGISS Tech. Rep.,* 95–12.

Yuan, T., Hyndman, R.D., Spence, G.D., and Desmons, B., 1996. Seismic velocity increase and deep-sea gas hydrate concentration above a bottom-simulating reflector on the northern Cascadia Continental Slope. *J. Geophys. Res.,* 101:13655–13671.

Ms 167IR-113

Table 14. Concentrations of inorganic carbon, calcium carbonate, total carbon, total organic carbon, total nitrogen, and total sulfur in weight percent (wt%) in Hole 1019C.

Core, section, interval (cm)	Depth (mbsf)	Inorganic carbon (wt%)	$CaCO_3$ (wt%)	Total carbon (wt%)	Total organic carbon (wt%)	Total nitrogen (wt%)	Total sulfur (wt%)	Total organic carbon/ total nitrogen
167-1019C-								
1H-1, 29–30	0.29	0.16	1.33	2.34	2.18	0.25	0.41	8.7
1H-3, 28–29	3.28	0.44	3.67	1.76	1.32	0.16	0.3	8.3
1H-5, 28–29	6.28	0.60	5.00	1.92	1.32	0.15	0.41	8.8
2H-1, 56–57	8.86	0.65	5.41	1.56	0.91	0.07	1.88	13.0
2H-3, 29–30	11.59	0.54	4.50	1.54	1.00	0.10	0.00	10.0
2H-5, 29–30	14.59	0.46	3.83	1.35	0.89	0.12	0.00	7.4
2H-7, 29–30	17.09	0.85	7.08	2.23	1.38	0.20	0.46	6.9
3H-2, 29–30	19.59	0.72	6.00	1.62	0.90	0.10	0.17	9.0
3H-4, 29–30	22.59	0.32	2.67	1.19	0.87	0.10	0.49	8.7
3H-5, 29–30	24.09	0.32	2.67	1.11	0.79	0.13	0.54	6.1

Only part of this table is produced here. The entire table appears on CD-ROM (back pocket).

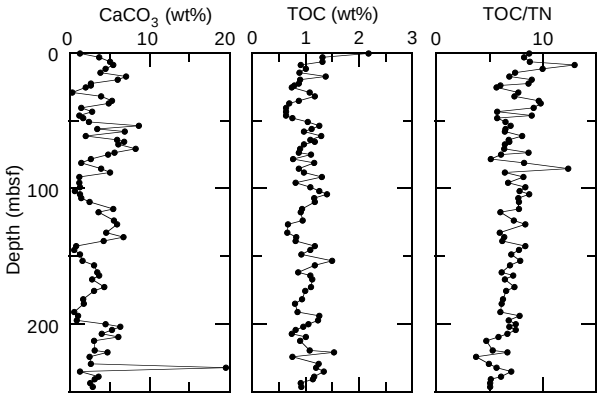

Figure 14. Depth variations of calcium carbonate, total organic carbon (TOC), and total organic carbon/total nitrogen (TOC/TN) ratios in sediments of Hole 1019C.

NOTE: For all sites drilled, core-description forms ("barrel sheets") and core photographs can be found in Section 3, beginning on page 499. Smear-slide data can be found in Section 4, beginning on page 1327. See Table of Contents for material contained on CD-ROM.

Table 15. The abundances of U^{k}_{37}' values, calculated SSTs, $C_{37:2}$ and $C_{37:3}$ alkenones, calcium carbonate, total organic carbon, and total nitrogen contents in selected samples from Hole 1019C.

Core, section, interval (cm)	Depth (mbsf)	U^{k}_{37}'	SST (°C)	$C_{37:3}$ (µg/g-rock)	$C_{37:2}$ (µg/g-rock)	C_{37} (µg/g-rock)	$CaCO_3$ (wt%)	TOC (wt%)	TN (wt%)	TOC/TN
167-1019C-										
1H-1, 35–37	0.35	0.46	12.3	0.23	0.19	0.42	1.58	1.89	0.24	7.88
1H-1, 110–112	1.10	0.43	11.4	0.20	0.15	0.36	2.33	1.84	0.23	8.00
1H-2, 35–37	1.85	0.43	11.6	0.13	0.10	0.23	2.00	1.42	0.23	6.17
1H-2, 110–112	2.60	0.47	12.8	0.06	0.05	0.11	2.17	1.43	0.18	7.94
1H-3, 35–37	3.35	0.49	13.3	0.17	0.16	0.33	2.08	1.44	0.12	12.00
1H-3, 110–112	4.10	0.55	15.0	0.17	0.21	0.38	4.33	1.53	0.25	6.12
1H-4, 35–37	4.85	0.48	12.9	0.31	0.29	0.60	3.42	1.73	0.96	1.80
1H-4, 110–112	5.60	0.44	11.8	0.23	0.18	0.41	3.17	1.15	0.14	8.21
1H-5, 35–37	6.35	0.52	14.2	0.16	0.18	0.34	5.08	1.18	0.15	7.87
1H-5, 110–112	7.10	0.56	15.4	0.13	0.17	0.30	7.92	1.71	0.20	8.55
1H-6, 35–37	7.85	0.35	9.16	0.15	0.08	0.23	4.50	0.97	0.10	9.70
2H-1, 35–37	8.65	0.45	12.2	0.15	0.12	0.28	5.67	0.95	0.10	9.50
2H-2, 35–37	10.15	0.49	13.2	0.13	0.12	0.26	4.92	1.04	0.19	5.47
2H-2, 110–112	10.90	0.42	11.1	0.14	0.10	0.23	1.92	0.63	0.06	10.50
2H-3, 35–37	11.65	0.36	9.53	0.31	0.18	0.49	4.50	1.11	0.16	6.94
2H-3, 110–112	12.40	0.35	9.22	0.14	0.08	0.22	4.08	0.76	0.08	9.50
2H-4, 35–37	13.15	0.36	9.47	0.13	0.07	0.20	4.75	0.83	0.14	5.93
2H-4, 110–112	13.90	0.53	14.6	0.19	0.22	0.41	4.67	1.21	0.11	11.00
2H-5, 35–37	14.65	0.38	9.99	0.11	0.07	0.18	3.83	0.87	0.09	9.67
2H-5, 110–112	15.40	0.37	9.78	0.14	0.08	0.23	5.08	0.49	0.07	7.00
2H-6, 35–37	16.15	0.42	11.3	0.15	0.11	0.25	4.50	0.94	0.09	10.44
2H-7, 35–37	17.15	0.42	11.2	0.37	0.27	0.64	6.17	1.24	0.19	6.53
3H-1, 35–37	18.15	0.41	10.9	0.17	0.12	0.28	5.00	1.02	0.12	8.50
3H-1, 105–107	18.85	0.39	10.4	0.17	0.11	0.29	5.83	1.07	0.14	7.64
3H-2, 35–37	19.65	0.43	11.5	0.20	0.15	0.34	5.00	0.84	0.14	6.00
3H-2, 110–112	20.40	0.39	10.2	0.18	0.11	0.29	4.25	0.83	0.08	10.38
3H-3, 35–37	21.15	0.42	11.3	0.22	0.16	0.39	5.83	0.76	0.12	6.33
3H-3, 110–112	21.90	0.41	11.0	0.29	0.20	0.49	5.33	0.77	0.06	12.83
3H-4, 35–37	22.65	0.43	11.6	0.18	0.14	0.31	2.42	0.89	0.08	11.13
3H-5, 35–37	24.15	0.52	14.0	0.12	0.13	0.25	5.42	0.83	0.06	13.83
3H-6, 25–27	25.55	0.44	11.8	0.20	0.16	0.36	2.00	0.73	0.07	10.43
3H-7, 20–22	27.00	0.48	13.0	0.14	0.13	0.27	1.42	0.57	0.05	11.40

Note: SST = sea-surface temperature.

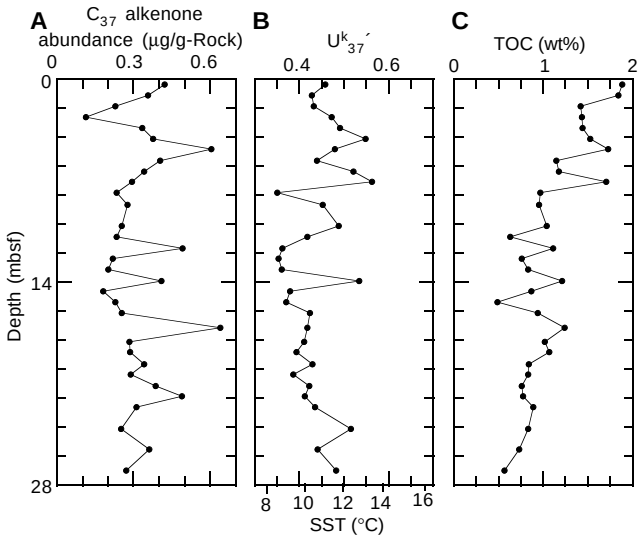

Figure 15. Depth variations of (**A**) C_{37} alkenone abundance, (**B**) U^{k}_{37}' value and calculated SST, and (**C**) total organic carbon (TOC) content in sediments of Hole 1019C.

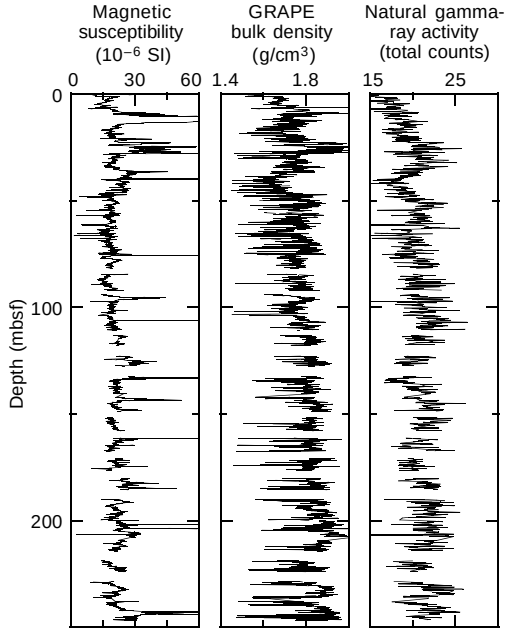

Figure 16. MST data from Hole 1019C.

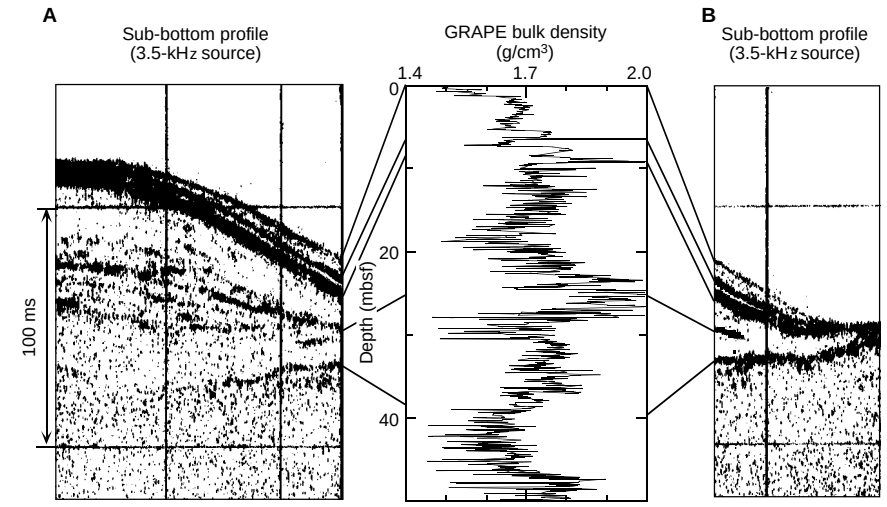

Figure 17. GRAPE bulk density vs. depth (mbsf) compared to the 3.5-kHz sub-bottom profiles. The two seismic reflection profiles (shown in **A** and **B**) are continuous, with the break placed at the location of Site 1019.

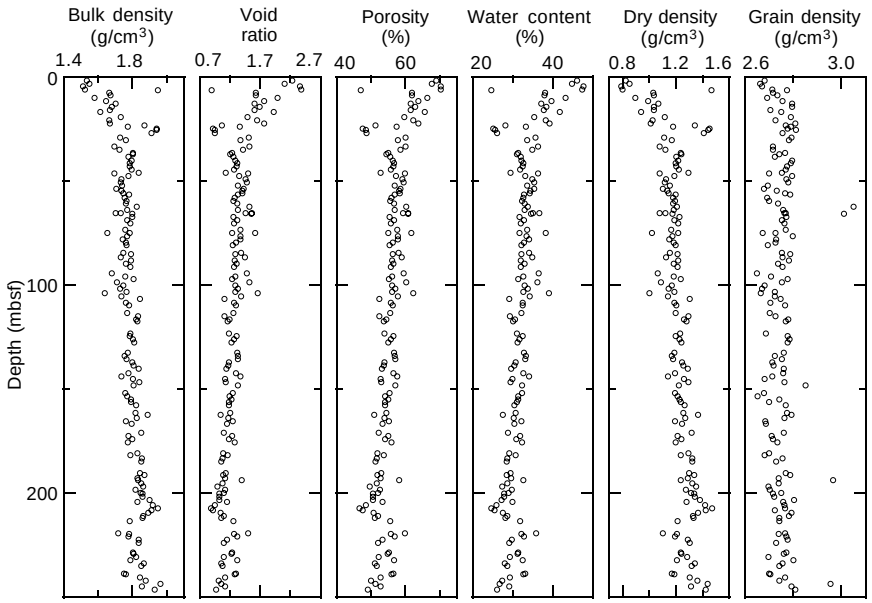

Figure 18. Index property data from Hole 1019C.

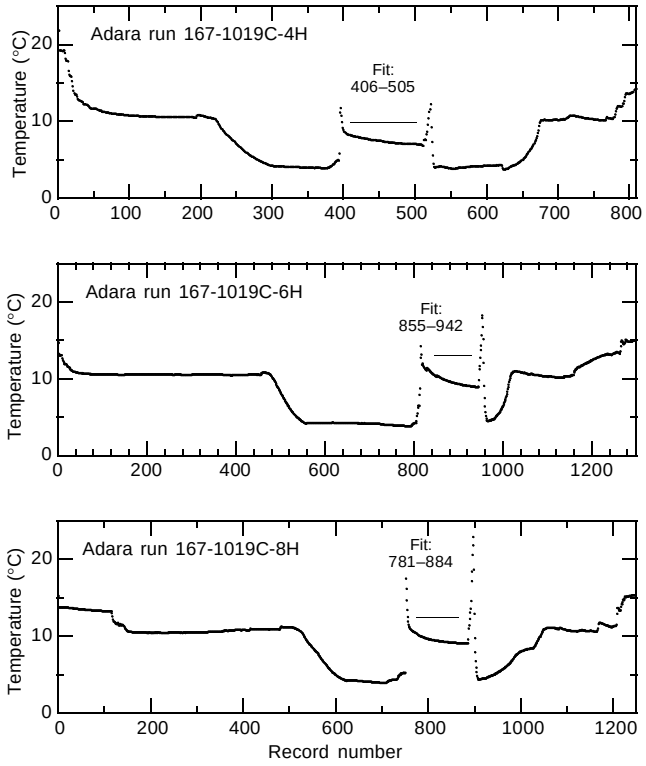

Figure 19. Hole 1019C downhole temperature vs. record number (5-s recording frequency) for each measurement run, showing the intervals fitted to determine the downhole temperature.

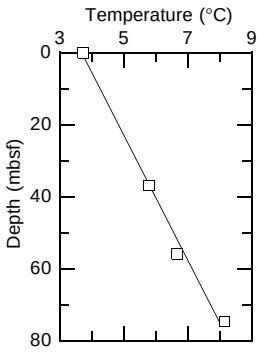

Figure 20. Downhole temperature gradient for Hole 1019C.

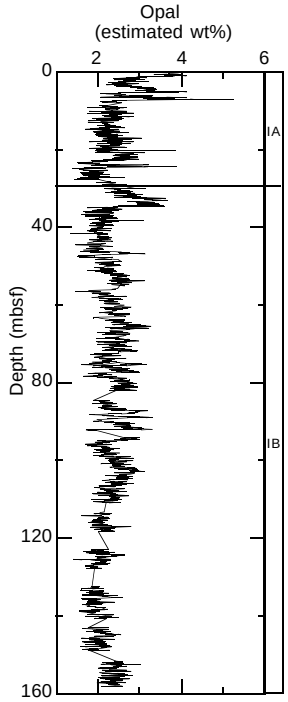

Figure 21. Predicted opal content for Hole 1019C based on site-survey color reflectance and opal data.

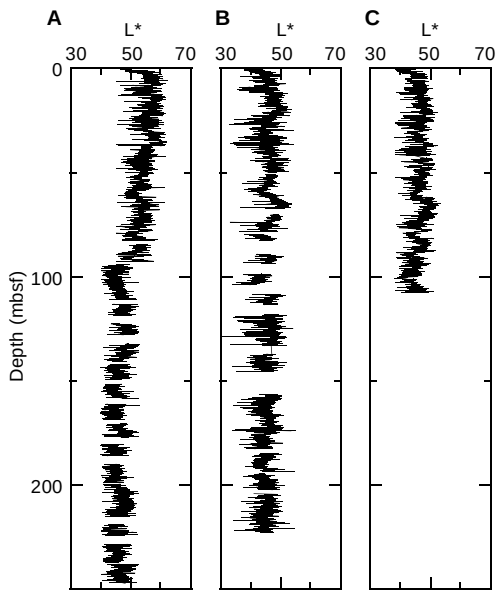

Figure 22. Intensity of sediment color CIELAB L* derived from digital color video images from Holes (**A**) 1019C, (**B**) 1019D, and (**C**) 1019E.

Table 18. Downhole measurements in Hole 1019C.

Date, time	Description
30 May 1996	
1500	Set pipe in Hole 1019C at 65 mbsf, wireline rig up, RIH density-porosity combination tool string, seas calm (1-m swell).
1700	Density-porosity tool string at TD, wireline heave compensator on, begin pass 1 (233–92 mbsf) at 300 m/hr. Continue logging to mudline and POOH.
2000	Rig down density-porosity tool string, rig up sonic-FMS tool string, RIH.
2045	Sonic-FM tool string at TD, wireline heave compensator on, begin pass 1 (228–82 mbsf) at 300 m/hr.
2130	Sonic-FM tool string at TD, begin pass 2 (226–60 mbsf). POOH sonic-FMS.
2300	Rig down sonic-FM, rig up GHMT tool string, RIH.
2345	GHMT tool string at TD, wireline heave compensator on, begin pass 1 (222–58 mbsf) at 1000 m/hr.
31 May 1996	
0015	GHMT tool string at TD, begin pass 2 (222–70 mbsf).
0030	POOH GHMT tool string, rig down wireline, end logging operations.

Note: RIH = run in hole, TD = total depth, FMS = formation microscanner, POOH = pull out of hole, GHMT = geological high-sensitivity magnetic tool.

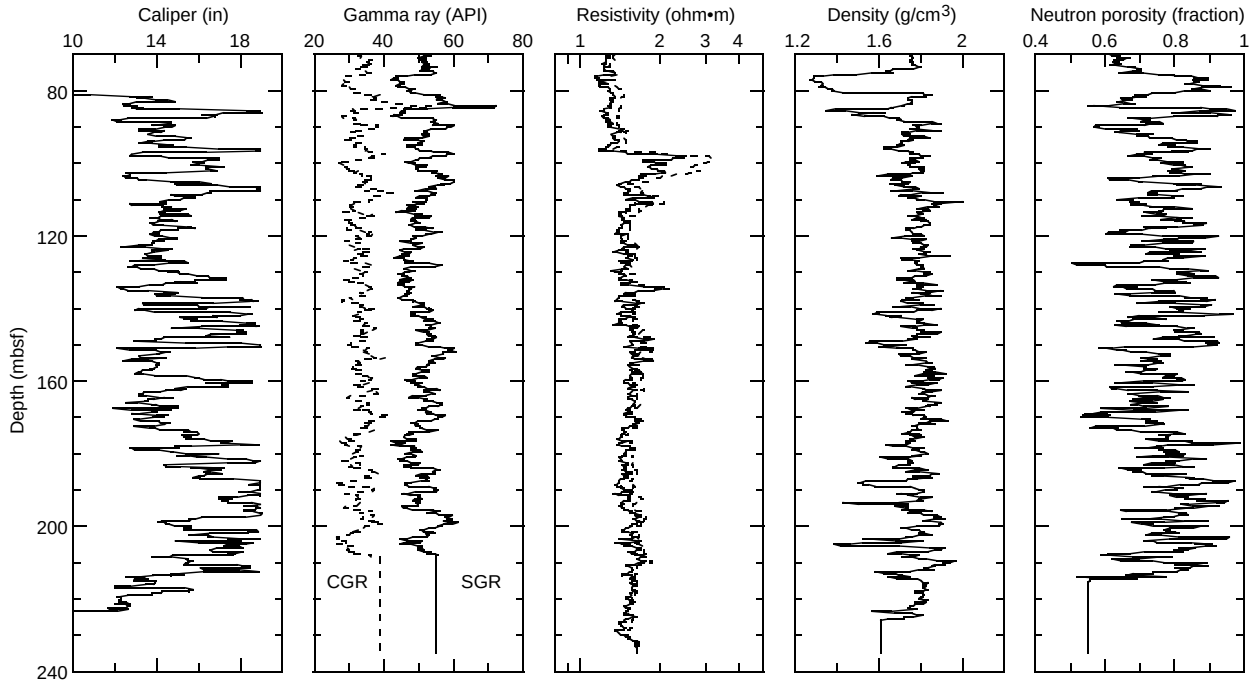

Figure 23. Downhole log data from the density-porosity combination tool string (pass 1) at Hole 1019C. The very irregular caliper curve indicates poor borehole conditions.

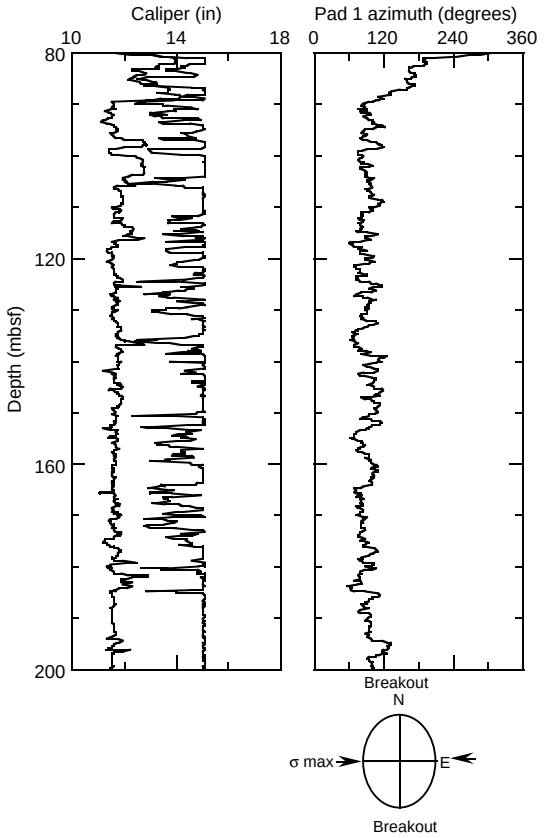

Figure 24. Comparison of orthogonal caliper measurements in Hole 1019C.

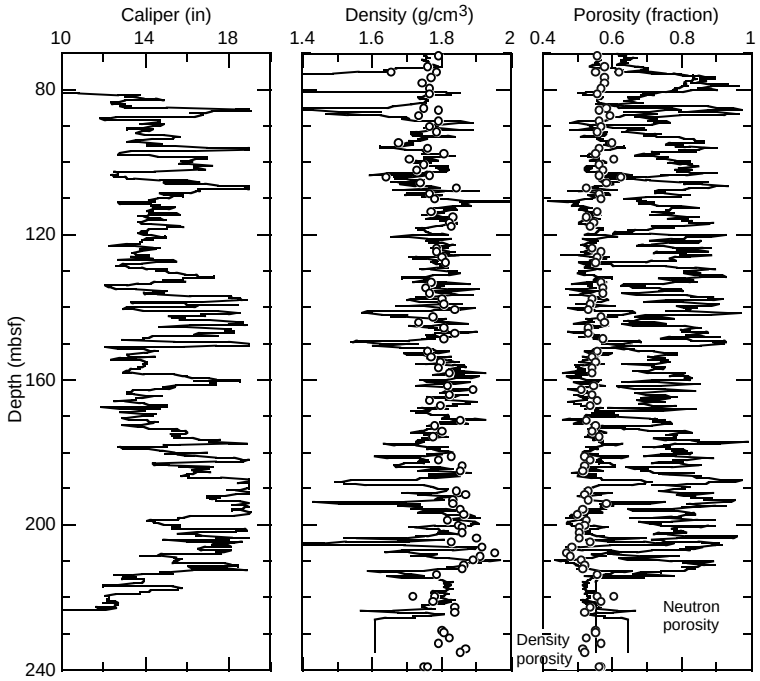

Figure 25. Comparison of core (open symbols) and log (line) physical properties data.

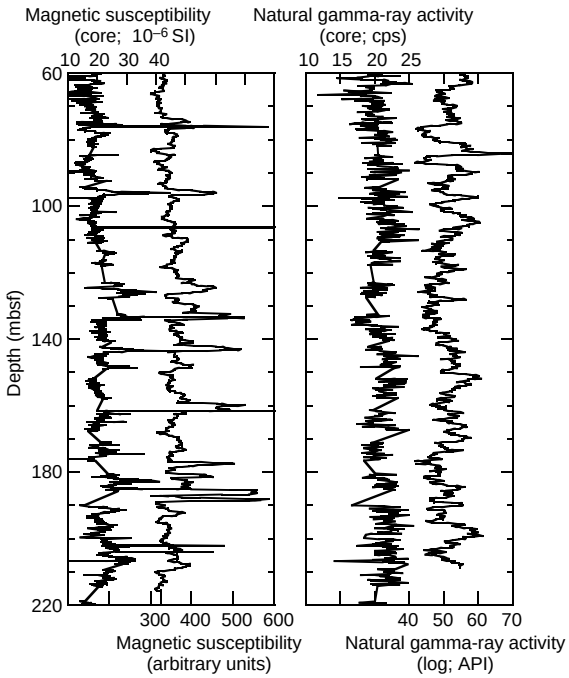

Figure 26. Comparison of core (MST) magnetic susceptibility and natural gamma activity data to equivalent log measurements (SUMT and HSGR, respectively). Log susceptibility values are uncalibrated.

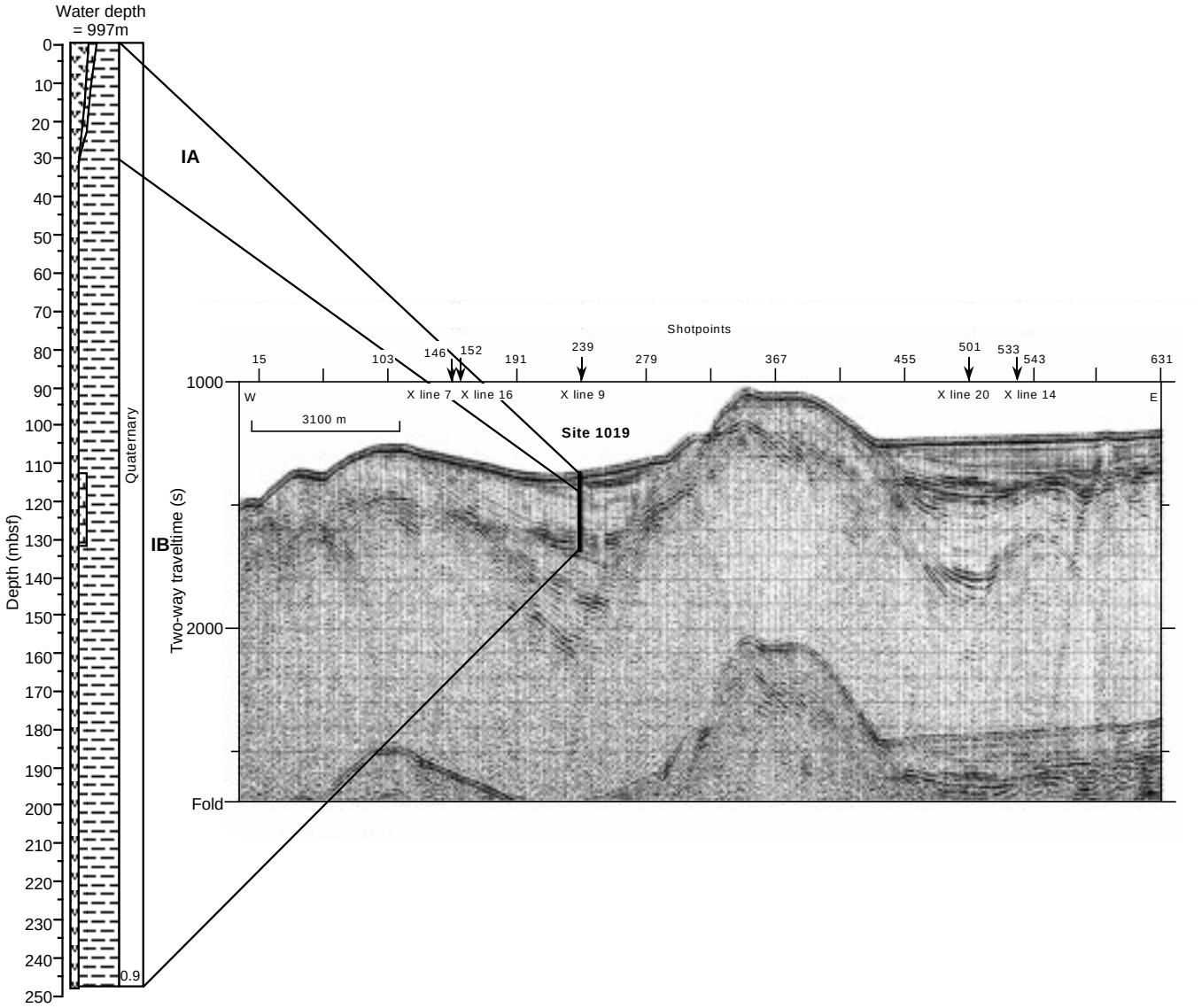

Figure 27. Comparison of the lithostratigraphic column at Site 1019 and a seismic reflection profile through it (Line W9406 CA1-12; Lyle et al., 1995a, 1995b). Ties are calculated from the few shipboard velocities and depth-time correlations between the 3.5 kHz sub-bottom profile and turbidites in the top of the sediment column (see “Physical Properties” section, this chapter). On y-axis, (s) = milliseconds.

SHORE-BASED LOG PROCESSING

HOLE 1019C

Bottom felt: 988.2 mbrf
Total penetration: 247.8 mbsf
Total core recovered: 214 m (86%)

Logging Runs

Logging string 1: DIT/HLDT/APS/HNGS
Logging string 2: FMS/GPIT/SDT/NGT (2 passes)
Logging string 3: GHMT/NGT (2 passes)
Wireline heave compensator was used to counter ship heave.

Bottom-Hole Assembly

The following bottom-hole assembly depths are as they appear on the logs after differential depth shift (see "Depth shift" section) and depth shift to the seafloor. As such, there might be a discrepancy with the original depths given by the drillers on board ship. Possible reasons for depth discrepancies are ship heave, use of wireline heave compensator, and drill string and/or wireline stretch.

DIT/HLDT/APS/HNGS: Bottom-hole assembly at ~44 mbsf.
FMS/GPIT/SDT/NGT: Did not reach bottom-hole assembly.
GHMT/NGT: Bottom-hole assembly at ~44 mbsf (pass 2).

Processing

Depth shift: Original logs have been interactively depth shifted with reference to HNGS from DIT/HLDT/APS/HNGS run and to the seafloor (–991 m). Pass 2 of the GHMT and FMS tool strings have been depth shifted with reference to Pass 1 of the same tool string, by using caliper and magnetic data for correlation. The amount of depth shift to seafloor corresponds to the water depth as observed on the logs and differs 2.8 m from the "bottom felt" depth given by the drillers.

Gamma-ray and environmental corrections: Corrections for borehole size and type of drilling fluid were performed on the NGT data from the FMS/GPIT/SDT/NGT and GHMT/NGT tool strings. HNGS data from the DIT/HLDT/APS/HNGS tool string were corrected in real-time during the recording.

Acoustic data processing: The array sonic tool was operated in standard depth-derived, borehole compensated, long spacing (8-10-10-12 ft) and short spacing (3-5-5-7 ft) mode. Because of the poor quality of the transit times caused by the degraded hole conditions, no standard processing has been performed. An uncompensated velocity value has been computed from the edited LTT4 (10-ft spacing) channel.

Quality Control

Data recorded through bottom-hole assembly, such as the HNGS and APS data above 44 mbsf, should be used qualitatively only because of the attenuation on the incoming signal.

Hole diameter was recorded by the hydraulic caliper on the HLDT tool (CALI) and the caliper on the FMS string (C1 and C2).

Note: Details of standard shore-based processing procedures are found in the "Explanatory Notes" chapter, this volume. For further information about the logs, please contact:

Cristina Broglia
Phone: 914-365-8343
Fax: 914-365-3182
E-mail: chris@ldeo.columbia.edu

Zhiping Tu
Phone: 914-365-8336
Fax: 914-365-3182
E-mail: ztu@ldeo.columbia.edu

Hole 1019C: Natural Gamma Ray-Density-Porosity Logging Data

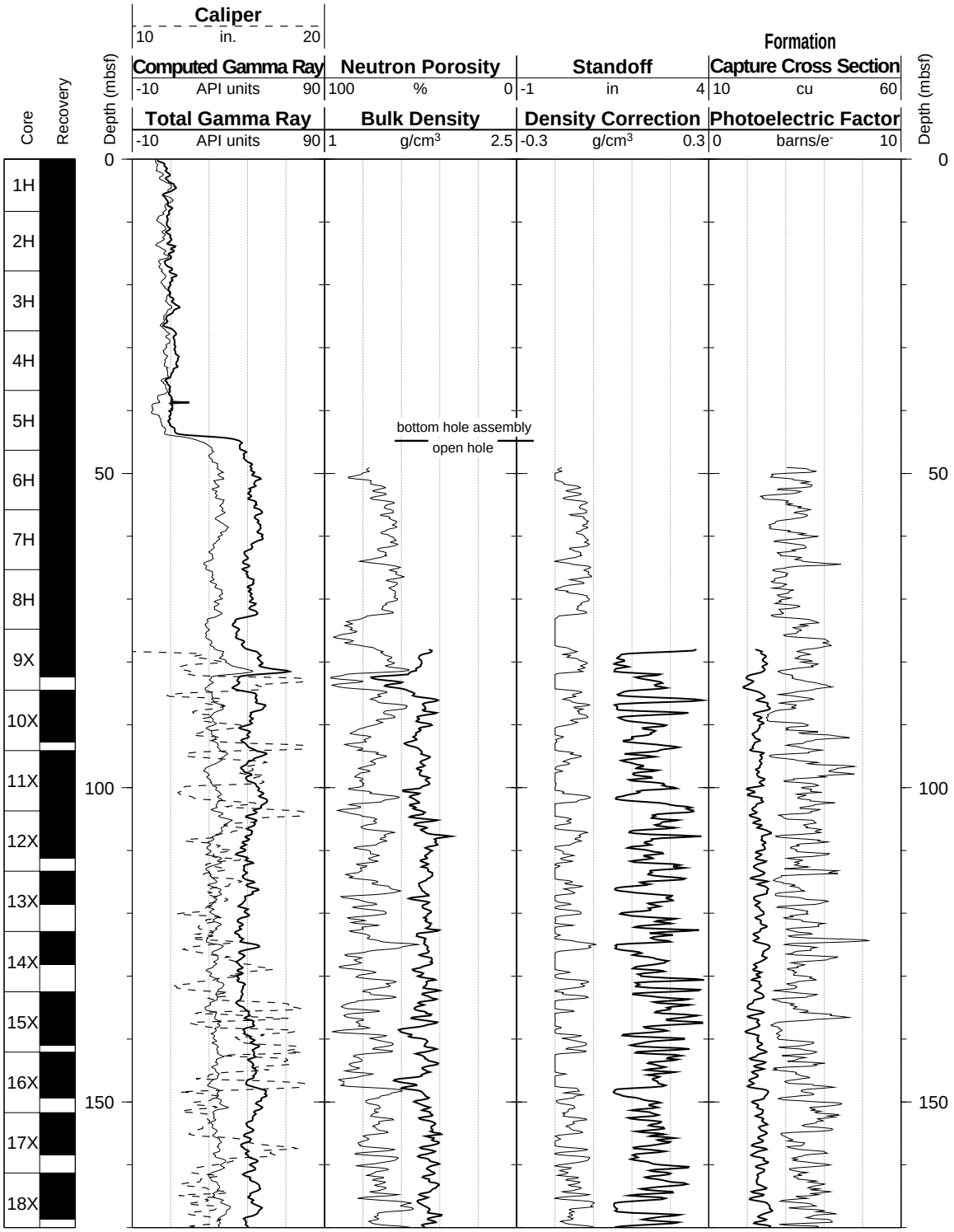

Hole 1019C: Natural Gamma Ray-Density-Porosity Logging Data (cont.)

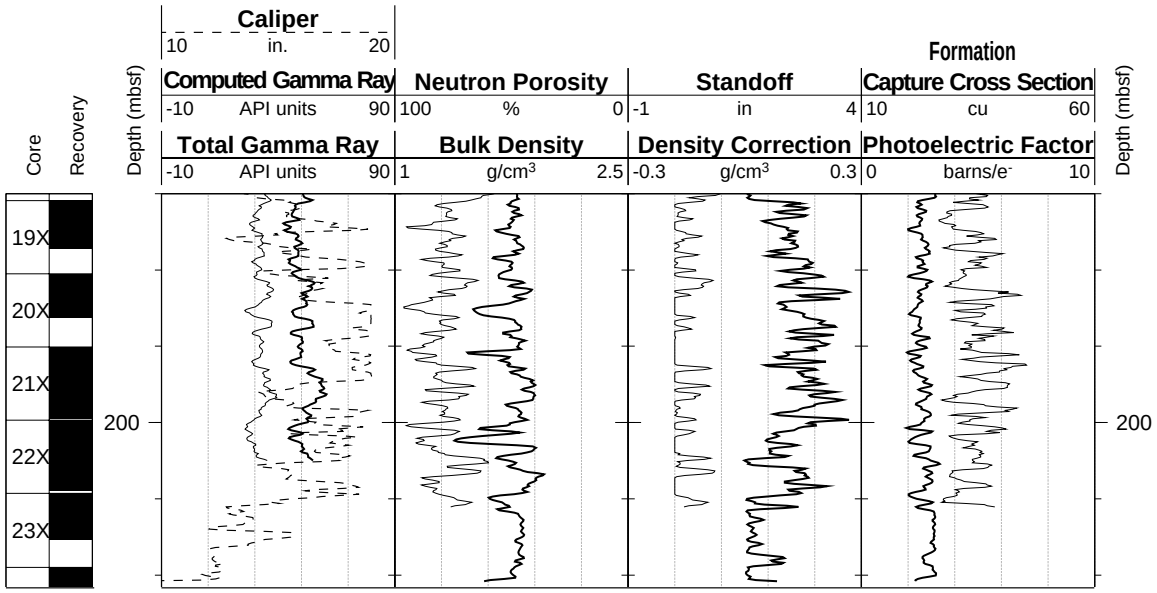

Hole 1019C: Natural Gamma Ray-Resistivity-Sonic Logging Data

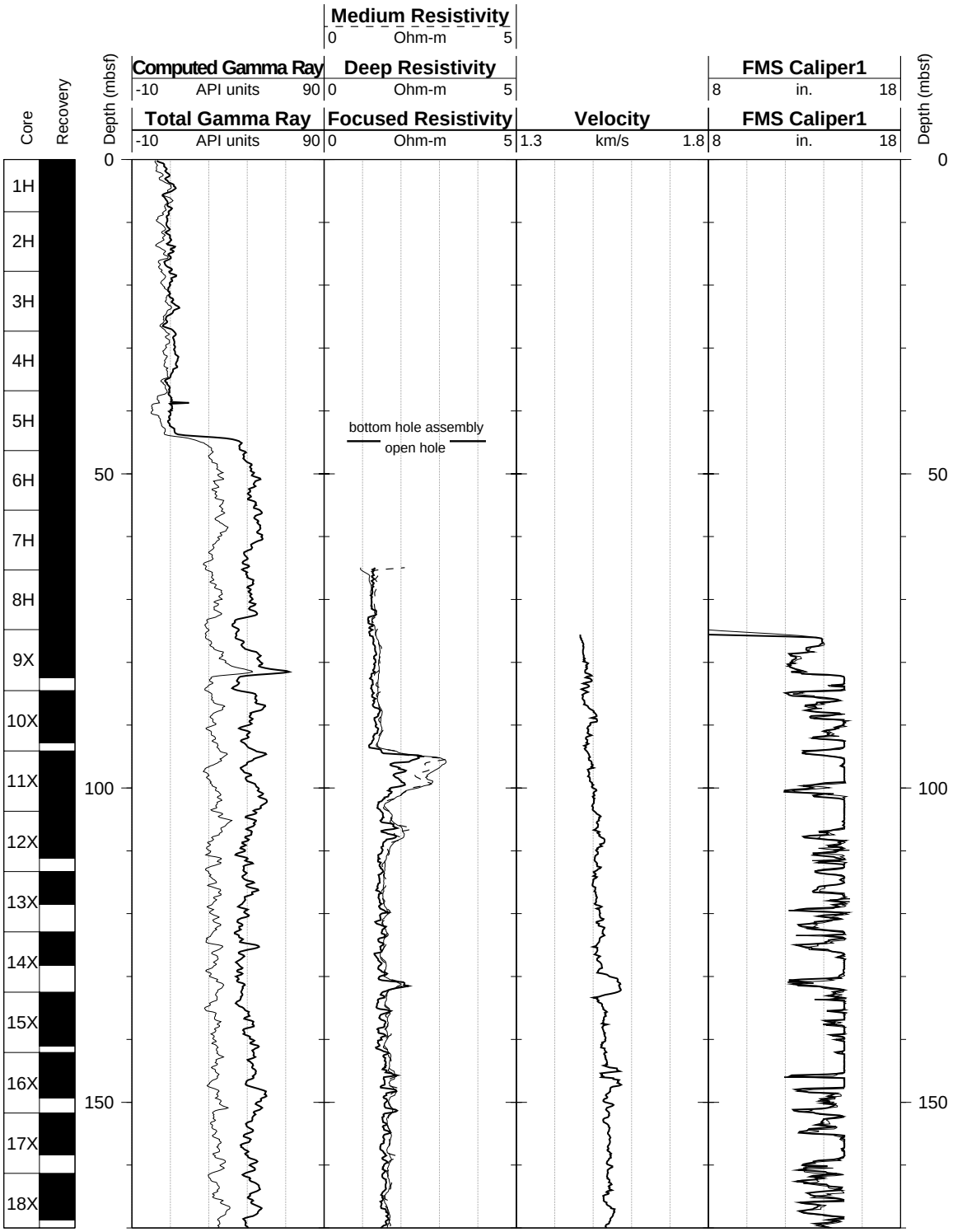

Hole 1019C: Natural Gamma Ray-Resistivity-Sonic Logging Data (cont.)

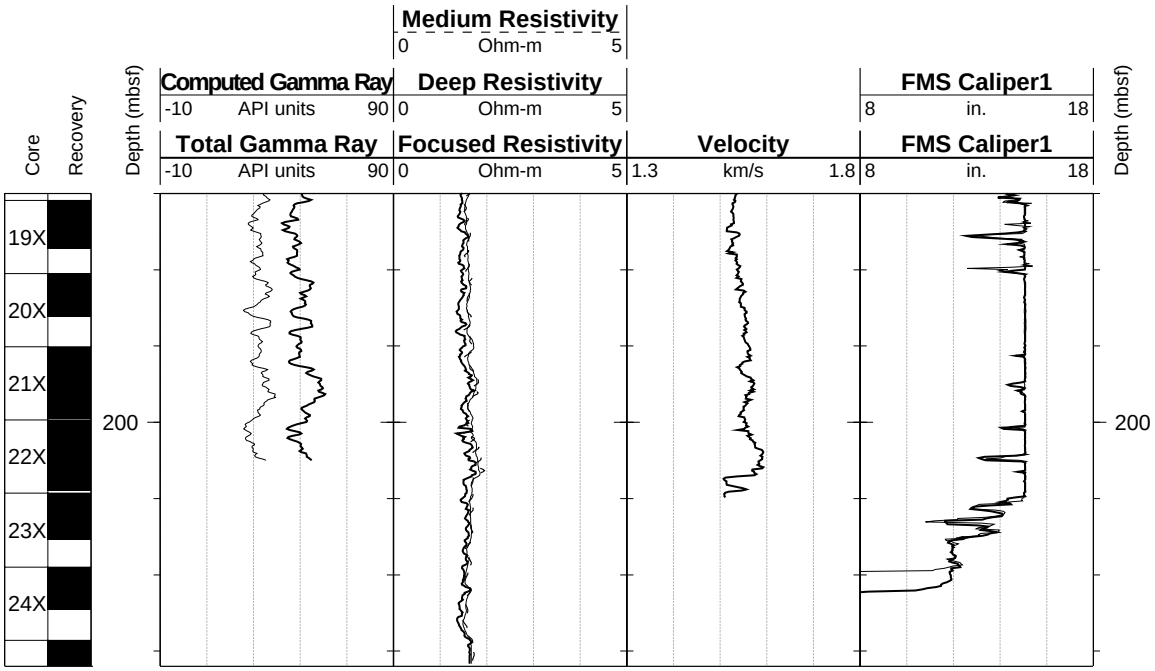

Hole 1019C: Natural Gamma Ray Logging Data

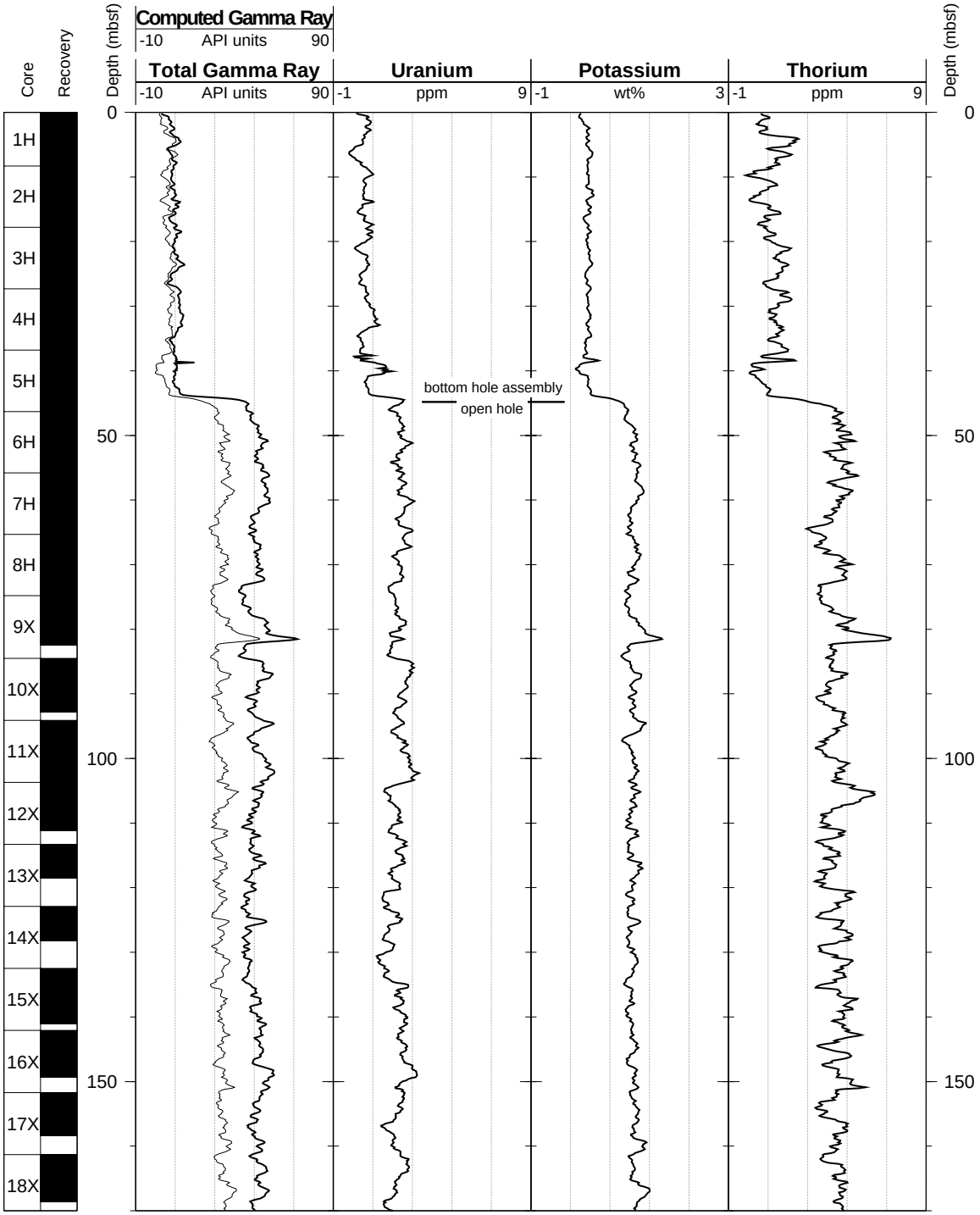

Hole 1019C: Natural Gamma Ray Logging Data (cont.)